Theor. Comput. Fluid Dyn. (2018) 32:537–560
https://doi.org/10.1007/s00162-018-0463-3

ORIGINAL ARTICLE

Xiaogang Yang · Yuezheng Gong · Jun Li · Jia Zhao · Qi Wang

On hydrodynamic phase field models for binary fluid mixtures

Received: 17 March 2017 / Accepted: 2 May 2018 / Published online: 24 May 2018

Abstract Two classes of thermodynamically consistent hydrodynamic phase field models have been developed for binary fluid mixtures of incompressible viscous fluids of possibly different densities and viscosities. One is quasi-incompressible, while the other is incompressible. For the same binary fluid mixture of two incompressible viscous fluid components, which one is more appropriate? To answer this question, we conduct a comparative study in this paper. First, we visit their derivation, conservation and energy dissipation properties and show that the quasi-incompressible model conserves both mass and linear momentum, while the incompressible one does not. We then show that the quasi-incompressible model is sensitive to the density deviation of the fluid components, while the incompressible model is not in a linear stability analysis. Second, we conduct a numerical investigation on coarsening or coalescent dynamics of protuberances using the two models. We find that they can predict quite different transient dynamics depending on the initial conditions and the density difference although they predict essentially the same quasi-steady results in some cases. This study

Communicated by S. Balachandar.

X. Yang
School of Science, Wuhan Institute of Technology, Wuhan 430205, Hubei Province, People's Republic of China
E-mail: xgyang@wit.edu.cn

Y. Gong
College of Science, Nanjing University of Aeronautics and Astronautics, Nanjing 210016, People's Republic of China
E-mail: gongyuezheng@nuaa.edu.cn

J. Li
School of Mathematical Sciences, Tianjin Normal University, Tianjin 300387, People's Republic of China
E-mail: nkjunli@foxmail.com

J. Zhao
Department of Mathematics & Statistics, Utah State University, Logan, UT 84322, USA
E-mail: jia.zhao@usu.edu

Q. Wang (✉)
Beijing Computational Science Research Center, Beijing 100093, People's Republic of China
E-mail: qwang@csrc.ac.cn

Q. Wang
Department of Mathematics, University of South Carolina, Columbia, SC 29028, USA

Q. Wang
School of Materials Science and Engineering, Nankai University, Tiajin 300350, People's Republic of China

thus cast a doubt on the applicability of the incompressible model to describe dynamics of binary mixtures of two incompressible viscous fluids especially when the two fluid components have a large density deviation.

Keywords Hydrodynamic phase field models · Quasi-incompressible models · Incompressible models · Viscous fluid mixtures · Density differences

1 Introduction

Phase field models have been successfully used to describe dynamics of flows of fluid mixtures of two or more fluid components, composite solid materials of different solid components, multiphase materials and complex biological systems for theoretical studies and numerical simulations [6,8–11,13,14,20–23,26,30,31,33–37]. When applied to flowing material systems, phase field models belong to a class of multiphase fluid models known as the one fluid multi-component model [7]. In this class of fluid models, an average velocity field is commonly used. However, in most phase field models for mixtures of incompressible fluids, a divergence free velocity field is used to describe the average flow field [29,32], whose physical identity is often vaguely delineated [3]. In some models, for instance, the mass-average velocity is employed [24,27,29], while in the others the volume-average velocity is used [3]. In fact, no matter if the velocity is a mass-average or a volume-average velocity [3], so long as a divergence free condition on the velocity is imposed in the model for fluid mixtures of different densities in their components, the governing system of equations can hardly be thermodynamically consistent while in the meantime the mass and momentum conservation laws are respected. This fact will become apparent when we go through the derivation of the binary hydrodynamic phase field theories in Sect. 2 in this paper.

One scientific question is what is the appropriate or "correct" hydrodynamic model for flows of fluid mixtures of incompressible fluid components that is not only thermodynamically but also hydrodynamically consistent, namely it respects the conservation laws in mass, linear and angular momentum and possesses energy dissipation properties. This motivates us to conduct the current comparative study between two classes of thermodynamically consistent hydrodynamic theories developed recently, using the binary fluid mixture system as an example. To study a binary fluid mixture with a small density difference, an early practice was to use a Boussinesq approximation, where the small density difference is neglected except for its effect in the gravitational force [25]. This approach, however, is not valid for large density deviations. For large density deviations, several quasi-incompressible phase field models have been developed [3,4,9,11,24,27–29], in which the models in [3,28] considered phenomenological modifications of the momentum equation. The thermodynamically consistent versions were investigated analytically in [1,2], where existence of strong local-in-time solutions and weak solutions was shown. Benchmark computations for the models in [3,9,11] were carried out by Aland and Voigt [5]. In [19], a numerical method that preserves a discrete energy law is developed for the quasi-incompressible model of [27], in which the mass fraction is used as the phase variable. Recently, the quasi-incompressible model for binary fluid flows with different densities using volume fractions as phase variables is developed by Shen et al. [29] and Aki et al. [4], and for multiphase fluid flows by Li and Wang [24]. An efficient, linear, second-order fully discrete scheme is also developed for the model to compare with incompressible models [16]. An alternative approach was taken to modify the compressible model into an incompressible version [3], where the momentum equation is approximated using the volume-average velocity instead of the mass-averaged velocity. The model has been studied numerically in [15,17,18], where the numerical methods developed are shown to be energy stable.

In summary, for large density deviations in the fluid mixture, there exist two classes of hydrodynamic phase field models: the quasi-incompressible one and the incompressible one, both of which satisfy their respective energy dissipation laws, i.e., they are thermodynamically consistent. More importantly, both are designed to describe hydrodynamics of the same physical fluid mixture. But, apparently, they are different in their mathematical structures. So, which one is more appropriate or correct? Can both be correct but with different mathematical structures? An affirmative answer is highly unlikely. Hence, a comprehensive evaluation of the two classes of hydrodynamic models becomes necessary and important. In this study, we will go over the derivation, analyze and numerically investigate the two models to evaluate them quantitatively and try to provide an answer to the question of which one is more appropriate. We focus on the incompressible model given in [15,17,18] and the quasi-incompressible model derived in [24,29].

Looking forward, we note that both models satisfy energy dissipation laws, but with different energy dissipation rates. This has already hinted that transient dynamics of the two models are going to be different.

Tracing back to the definition of the kinetic energy in the two models, we notice that the kinetic energy in the incompressible model is not the "real" kinetic energy since it is defined using the volume-average velocity. In addition, we point it out that the incompressible model does not satisfy the linear momentum balance law. These discrepancies between the models perhaps contribute to the difference in model predictions in the numerical experiments that we show in the paper as well as the linear analysis. In particular, the linear stability analysis of the two models reveals that the unstable growth rate in the quasi-incompressible model depends on the density ratio (or density difference) of the two constituent components while it is completely independent of it in the incompressible model. Analogously, the transient dynamics of the quasi-incompressible model varies with respect to the density difference while the incompressible model is insensitive to the difference. Based on the conservation laws that the models satisfy and the ad hoc definition of the kinetic energy in the incompressible model, the outcome of this study clearly favors the quasi-incompressible model especially when the density difference is large. When the density difference is small, dynamics predicted by both models are not too far apart though, hinting the incompressible model perhaps can be used as an approximation just like one can use the Boussinesq approximation in this regime. Although both models are thermodynamically consistent in the sense that they possess their respective energy dissipation laws, given their differences in mathematical structures and the conservation laws that they satisfy, this study clearly selects the one that is more appropriate for the fluid mixture of viscous fluid components. Hopefully, this study will serve as a guide for people to choose the right model to use in the future. One lesson we learned from this study is that thermodynamically consistency is a nice mathematical pretext; it should never be used as a criterion to justify applicability of physical model; physical models must be derived the following pertinent physical laws.

The rest of the paper is organized as follows. In Sect. 2, we derive the two models using a generalized Onsager principle [24]. In Sect. 3, we compare the two models theoretically. In Sect. 4, we discuss linear stability of the models with respect to a constant steady state which is a solution of both models. In Sect. 5, we discuss transient dynamical predictions of the models in nonlinear regimes in one space dimension and time. Finally, we give the concluding remark.

2 Model derivation

We consider a binary fluid mixture consisting of two incompressible viscous fluid components with molecular number densities n_j, $j = 1, 2$, respectively. We assume that the molecule of the jth component has mass m_j and volume v_j, $j = 1, 2$. Then, the specific mass density of the jth component is $\hat{\rho}_j = \frac{m_j}{v_j}$. The mass density of the jth component in the mixture is $\rho_j = n_j m_j$. Then, the total mass density of the mixture is given by

$$\rho = n_1 m_1 + n_2 m_2 = \rho_1 + \rho_2. \tag{2.1}$$

The mass fraction s_j of the jth component in the binary mixture is defined by $s_j = \frac{\rho_j}{\rho}$, $j = 1, 2$, so that

$$s_1 + s_2 = 1. \tag{2.2}$$

The volume fraction c_j of the jth component in the mixture is defined by

$$c_j = n_j v_j = \frac{n_j m_j}{m_j/v_j} = \frac{\rho_j}{\hat{\rho}_j}, \quad j = 1, 2. \tag{2.3}$$

Because n_j is the number density, the total number of the molecules of the jth component in the unit volume, we have

$$c_1 + c_2 = 1. \tag{2.4}$$

Both (2.2) and (2.4) are valid in the mixture provided the excluded volumes of the molecules are unchanged after mixing, which is assumed in this paper.

The mass density of the binary fluid can be represented by the combination of the specific densities and the volume fractions:

$$\rho = c_1 \hat{\rho}_1 + c_2 \hat{\rho}_2. \tag{2.5}$$

The mass fraction and the volume fraction are related by the following relation

$$c_i = \frac{s_i \rho}{\hat{\rho}_i}, \, i = 1, 2. \tag{2.6}$$

2.1 Linear momentum versus the pseudo linear momentum

The linear momentum of fluid i is given by $\rho_i \mathbf{v}_i, i = 1, 2$. The total linear momentum density of the binary mixture is defined as the sum of that from each component:

$$\mathbf{p} = \rho_1 \mathbf{v}_1 + \rho_2 \mathbf{v}_2, \tag{2.7}$$

where $\mathbf{v}_j$ is the velocity of the jth component. From the definition of the linear momentum, the mass-averaged velocity $\mathbf{v}$ of the binary mixture is defined as

$$\mathbf{v} = \frac{\mathbf{p}}{\rho} = \frac{1}{\rho}(\rho_1 \mathbf{v}_1 + \rho_2 \mathbf{v}_2) = s_1 \mathbf{v}_1 + s_2 \mathbf{v}_2. \tag{2.8}$$

Using the volume fractions, we define the volume-averaged velocity $\mathbf{u}$ of the binary mixture as follows

$$\mathbf{u} = c_1 \mathbf{v}_1 + c_2 \mathbf{v}_2. \tag{2.9}$$

When the density of the two fluid components is distinct, the two average velocities are different! We next show how different it can be between the two linear momentum vectors defined by the two different velocity vectors.

For the volume-average velocity, we define the pseudo linear momentum vector as follows

$$\hat{\mathbf{p}} = \rho \mathbf{u} = \rho(c_1 \mathbf{v}_1 + c_2 \mathbf{v}_2). \tag{2.10}$$

The difference between the "real" linear momentum and the pseudo linear momentum is

$$\delta \mathbf{p} = \mathbf{p} - \hat{\mathbf{p}} = \rho(s_1 \mathbf{v}_1 + s_2 \mathbf{v}_2) - \rho(c_1 \mathbf{v}_1 + c_2 \mathbf{v}_2). \tag{2.11}$$

The mass fractions s_j can be expressed by the volume fractions and the specific mass densities as follows

$$s_j = \frac{\rho_j}{\rho} = \frac{n_j m_j}{n_1 m_1 + n_2 m_2} = \frac{c_j m_j / v_j}{c_1 m_1 / v_1 + c_2 m_2 / v_2} = \frac{c_j \hat{\rho}_j}{c_1 \hat{\rho}_1 + c_2 \hat{\rho}_2}. \tag{2.12}$$

Because $c_2 = 1 - c_1$, the momentum difference $\delta \mathbf{p}$ can be simplified into

$$\delta \mathbf{p} = \hat{\rho}_1 (\mathbf{v}_1 - \mathbf{v}_2) c_1 (1 - c_1) \left(1 - \frac{1}{r}\right), \tag{2.13}$$

where $r = \frac{\hat{\rho}_1}{\hat{\rho}_2}$ is the ratio of the specific mass densities. For $c_1 \in (0, 1)$, when either $\mathbf{v}_1 = \mathbf{v}_2$ or $r = 1 (\hat{\rho}_1 = \hat{\rho}_2)$, $\delta \mathbf{p} = 0$. Otherwise, $\delta \mathbf{p} \neq \mathbf{0}$. When $\delta \mathbf{p} \neq 0$, the difference may be far from zero. For instance, we assume the second fluid moves at a special velocity $\mathbf{v}_2 = s \mathbf{v}_1$, where s is a scalar. Then, the momentum difference is

$$\delta \mathbf{p} = \hat{\rho}_1 \mathbf{v}_1 (1 - s) c_1 (1 - c_1) \left(1 - \frac{1}{r}\right). \tag{2.14}$$

In order to show the difference clearly, we fix r and draw the graph of the coefficient function $d(c_1, r)$ defined by

$$d(c_1, r) = c_1 (1 - c_1) \left(1 - \frac{1}{r}\right), \quad c_1 \in [0, 1], r > 0. \tag{2.15}$$

Notice that $1 - \frac{1}{r} = \frac{(\hat{\rho}_1 - \hat{\rho}_2)}{\hat{\rho}_1}$. So, $d(c_1, r) \sim (\hat{\rho}_1 - \hat{\rho}_2)$ at fixed c_1. It is easy to see that when the density ratio r is far from 1, the absolute value of the coefficient function $d(c_1, r)$ is large at some value of c_1, as shown in Fig. 1. If we write the real linear momentum as

$$\mathbf{p} = \hat{\rho}_1 \mathbf{v}_1 \left(c_1 + s(1 - c_1) \frac{1}{r}\right), \tag{2.16}$$

the relative error: ratio of the linear momentum difference to the real linear momentum, is given by

$$re(s, c_1, r) = \frac{\|\delta \mathbf{p}\|}{\|\mathbf{p}\|} = \left| \frac{(1 - s) c_1 (1 - c_1) \left(1 - \frac{1}{r}\right)}{c_1 + s(1 - c_1) \frac{1}{r}} \right|. \tag{2.17}$$

In Fig. 2, it is easy to find that the relative error of the momentum is large (up to about 9%) when the density ratio r is far from 1. Figures 1 and 2 show the coefficient function and the relative error function at a few selected density ratios and s values for this special binary fluid mixture flow where $\mathbf{v}_2 = s \mathbf{v}_1$ is assumed. This indicates that the difference of the two linear momenta can indeed be quite significant for any given set of the composition and velocity field in each individual component in the mixture. This fact should not be easily ignored when one develops new theories for the binary mixture fluid flows since it can induce significant errors! We next recall the derivation of the two hydrodynamic phase field models, dissect what approximations are made during the derivation and examine their respective energy dissipation laws.

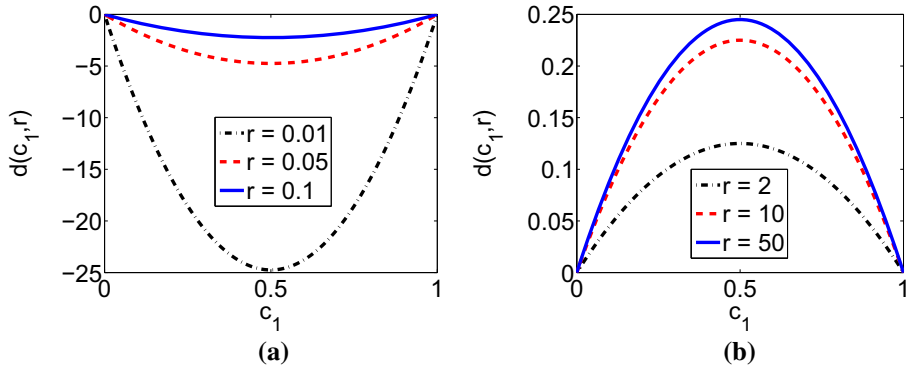

Fig. 1 Difference coefficient function $d(c_1, r)$ in the linear momentum. **a** $d(c_1, r), r < 1$. **b** $d(c_1, r), r > 1$

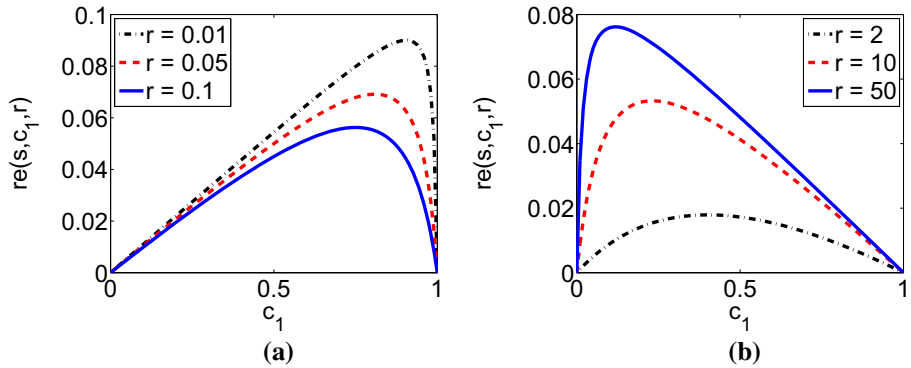

Fig. 2 Relative error $re(s, c_1, r)$ with fixed $s = 0.9$. **a** $re(s, c_1, r), r = 0.01, 0.05, 0.1 < 1, s = 0.9$. **b** $re(s, c_1, r), r = 2, 10, 50 > 1, s = 0.9$

2.2 Quasi-incompressible model (PFM)

We consider two incompressible viscous fluid components and recall that the mass conservation laws for the two incompressible fluid components are given, respectively, by

$$\partial_t \rho_1 + \nabla \cdot (\rho_1 \mathbf{v}_1) = 0, \qquad \partial_t \rho_2 + \nabla \cdot (\rho_2 \mathbf{v}_2) = 0.$$

The total mass is thus conserved

$$\partial_t \rho + \nabla \cdot (\rho \mathbf{v}) = 0. \tag{2.18}$$

The conservation law of the linear momentum is given by

$$\partial_t (\rho \mathbf{v}) + \nabla \cdot (\rho \mathbf{v}\mathbf{v}) = \nabla \cdot \sigma + \mathbf{F}_e, \tag{2.19}$$

where σ is the stress tensor and $\mathbf{F}_e$ is the elastic force, both of which will be determined by constitutive relations. We can add the external force (like gravity) if necessary. For fluid component 1, we rewrite the flux $(\rho \mathbf{v_1})$ into a convective part moving with the mass-average velocity $\mathbf{v}$ and a diffusive part associated to the relative flux between the two components:

$$\partial_t \rho_1 + \nabla \cdot (\rho_1 \mathbf{v} + \hat{\mathbf{j}}) = 0, \tag{2.20}$$

where $\hat{\mathbf{j}} = \frac{\rho_1 \rho_2 (\mathbf{v}_1 - \mathbf{v}_2)}{\rho}$ is the diffusive flux.

In the following, we denote the volume fraction of component 1 as $c = c_1 = \frac{\rho_1}{\hat{\rho}_1}$ and its excessive diffusive flux as $\mathbf{j} = \frac{\hat{\mathbf{j}}}{\hat{\rho}_1}$. The transport equation for c is obtained rom (2.20) and given by

$$\partial_t c + \nabla \cdot (c\mathbf{v} + \mathbf{j}) = 0. \tag{2.21}$$

The total mass conservation can be written as follows by using the transport equation of c together with the mass conservation equation,

$$\nabla \cdot \mathbf{v} = -\left(1 - \frac{\hat{\rho}_1}{\hat{\rho}_2}\right) \nabla \cdot \mathbf{j}. \tag{2.22}$$

This shows that as long as the density ratio between the two fluid component is not 1 or there exists the diffusive flux $\mathbf{j}$, the mass-average velocity field is not going to be divergence free.

We next assume the free energy of the binary fluid system in a fixed volume element V is prescribed as

$$F = F(c, \nabla c) = \int_V f(c, \nabla c) \mathrm{d}\mathbf{x},$$

where f is the free energy density. At the boundary of the fixed material domain ∂V, we assume there exists an interfacial free energy with density $g(c)$

$$G = G(c) = \int_{\partial V} g(c) \mathrm{d}S.$$

The total free energy of the system is given by

$$E^{\text{total}} = \int_V \left(\frac{\rho}{2} \|\mathbf{v}\|^2\right) \mathrm{d}\mathbf{x} + F + G. \tag{2.23}$$

The energy dissipation rate at a constant absolute temperature T is given by

$$\frac{\mathrm{d}E^{\text{total}}}{\mathrm{d}t} = \int_V \mathrm{d}\mathbf{x} \left\{\frac{1}{2} \frac{\partial(\rho \mathbf{v}^2)}{\partial t} + \frac{\partial f}{\partial t}\right\} + \int_{\partial V} \frac{\partial g}{\partial t} \mathrm{d}S. \tag{2.24}$$

There are three parts in the integration: the first and second parts are the rates of change in the kinetic energy and the system free energy, respectively. The third one is the rate of change in the surface free energy. The time rate of change in the free energy density is given by

$$\frac{\partial f}{\partial t} = \frac{\partial f}{\partial c} \frac{\partial c}{\partial t} + \frac{\partial f}{\partial (\nabla c)} \cdot \frac{\partial (\nabla c)}{\partial t} = \mu \frac{\partial c}{\partial t} + \nabla \cdot \left(\frac{\partial f}{\partial (\nabla c)} \frac{\partial c}{\partial t}\right). \tag{2.25}$$

The field conjugate to c is the chemical potential $\mu = \frac{\delta F}{\delta c} = \frac{\partial f}{\partial c} - \nabla \cdot \frac{\partial f}{\partial (\nabla c)}$. So the energy dissipation rate can be written as

$$\frac{\mathrm{d}E^{\text{total}}}{\mathrm{d}t} = \int_V \mathrm{d}\mathbf{x} \left\{\frac{1}{2} \frac{\partial(\rho \mathbf{v}^2)}{\partial t} + \mu \frac{\partial c}{\partial t}\right\} + \int_{\partial V} \mathrm{d}S \left\{\left(\frac{\partial f}{\partial (\nabla c)} \frac{\partial c}{\partial t}\right) \cdot \mathbf{n} + \frac{\partial g}{\partial c} \frac{\partial c}{\partial t}\right\}, \tag{2.26}$$

where ∂V is the surface of volume V and $\mathbf{n}$ is the external unit normal of ∂V. By using the transport equation of c, and the conservation of the total system mass and linear momentum, we have

$$\begin{aligned} \frac{\mathrm{d}E^{\text{total}}}{\mathrm{d}t} = &\int_V \mathrm{d}\mathbf{x} \{-\nabla \mathbf{v} : \sigma + \mathbf{v} \cdot (\mathbf{F}_e + c \nabla \mu) + \mathbf{j} \cdot \nabla \mu\} + \int_{\partial V} \mathrm{d}S \left\{\mathbf{v} \cdot \left(-\frac{1}{2} \rho \mathbf{v}^2 \mathbf{I} - c\mu \mathbf{I} + \sigma\right) \cdot \mathbf{n} \right. \\ &\left. -\mu \mathbf{j} \cdot \mathbf{n} + \left(\mathbf{n} \cdot \frac{\partial f}{\partial \nabla c} + \frac{\partial g}{\partial c}\right) \frac{\partial c}{\partial t}\right\}. \end{aligned} \tag{2.27}$$

If we assume

$$\mathbf{v}|_{\partial V} = 0, \quad \mathbf{j} \cdot \mathbf{n}\Big|_{\partial V} = 0, \quad \left[\mathbf{n} \cdot \frac{\partial f}{\partial \nabla c} + \frac{\partial g}{\partial c}\right]\Big|_{\partial V} = 0 \tag{2.28}$$

at the boundary, the last surface integral is zero. This is equivalent to say that dynamics at the surface does not contribute to energy dissipation of the binary fluid system. These define additional boundary conditions for the velocity and the internal variable c via the excessive flux. If the surface term is not assigned into zero, it may

contribute to the energy dissipation. The latter case includes moving boundaries, which we will not pursue in this study. We define the elastic force and the strain rate tensor as

$$\begin{aligned} \mathbf{F}_e &= -c\nabla\mu, \\ \mathbf{D} &= \frac{1}{2}(\nabla\mathbf{v} + \nabla\mathbf{v}^T). \end{aligned} \tag{2.29}$$

The total stress tensor σ is in fact symmetric that can be proved by the angular momentum conservation of the system. The energy dissipation is simplified into

$$\frac{\mathrm{d}E^{\text{total}}}{\mathrm{d}t} = \int_V \mathrm{d}\mathbf{x}\{-\mathbf{D} : \sigma + \mathbf{j}\cdot\nabla\mu\}. \tag{2.30}$$

In addition, the total stress can be written as $\sigma = \sigma^s - \Pi\mathbf{I}$, where Π is the hydrostatic pressure. Then, the energy dissipation rate is

$$\begin{aligned} \frac{\mathrm{d}E^{\text{total}}}{\mathrm{d}t} &= \int_V \mathrm{d}\mathbf{x}\left\{-\mathbf{D} : \sigma^s + \Pi\nabla\cdot\mathbf{v} + \mathbf{j}\cdot\nabla\mu\right\} \\ &= -\int_V \mathrm{d}\mathbf{x}\left\{\mathbf{D} : \sigma^s + \mathbf{j}\cdot\left(-\nabla\left(\mu + (1-\frac{\hat{\rho}_1}{\hat{\rho}_2})\Pi\right)\right)\right\}. \end{aligned} \tag{2.31}$$

Then, we propose the following constitutive relations:

$$\begin{aligned} \sigma^s &= 2\eta\mathbf{D} + \nu tr(\mathbf{D})\mathbf{I}, \\ \mathbf{j} &= -\lambda\nabla\left(\mu + \left(1 - \frac{\hat{\rho}_1}{\hat{\rho}_2}\right)\Pi\right), \end{aligned} \tag{2.32}$$

where η is the shear viscosity coefficient, ν is the volumetric viscosity, and λ is the mobility coefficient. Finally, the energy dissipation rate is shown as non-positive,

$$\frac{\mathrm{d}E^{\text{total}}}{\mathrm{d}t} = -\int_V \mathrm{d}\mathbf{x}\left\{2\eta\mathbf{D} : \mathbf{D} + \nu(tr(\mathbf{D}))^2 + \lambda\left\|\nabla\left(\mu + \left(1 - \frac{\hat{\rho}_1}{\hat{\rho}_2}\right)\Pi\right)\right\|^2\right\} \leq 0. \tag{2.33}$$

Clearly, the density ratio $\frac{\hat{\rho}_1}{\hat{\rho}_2}$ has an impact on the energy dissipation rate in this model.

We summarize the equations in the hydrodynamic phase field model with mass-average velocity (named PFM model) in the following,

$$\begin{aligned} &\partial_t c + \nabla\cdot(c\mathbf{v}) = \nabla\cdot\left(\lambda\nabla\left(\mu + \left(1 - \tfrac{\hat{\rho}_1}{\hat{\rho}_2}\right)\Pi\right)\right), \\ &\nabla\cdot\mathbf{v} = \left(1 - \tfrac{\hat{\rho}_1}{\hat{\rho}_2}\right)\nabla\cdot\left(\lambda\nabla\left(\mu + \left(1 - \tfrac{\hat{\rho}_1}{\hat{\rho}_2}\right)\Pi\right)\right) = \left(1 - \tfrac{\hat{\rho}_1}{\hat{\rho}_2}\right)(\partial_t c + \nabla\cdot(c\mathbf{v})), \\ &\rho = \left(\hat{\rho}_1 - \hat{\rho}_2\right)c + \hat{\rho}_2, \\ &\rho\left(\tfrac{\partial\mathbf{v}}{\partial t} + \mathbf{v}\cdot\nabla\mathbf{v}\right) = -\nabla\Pi + 2\nabla\cdot(\eta\mathbf{D}) + \nabla(\nu tr\mathbf{D}) - c\nabla\mu. \end{aligned} \tag{2.34}$$

The viscosity coefficients for the fluid mixture are interpolated through the volume fractions and given by

$$\eta = c\eta_1 + (1-c)\eta_2, \quad \nu = c\nu_1 + (1-c)\nu_2, \tag{2.35}$$

where $\eta_{1,2}$, $\nu_{1,2}$ are constant shear and volumetric viscosities for fluid component 1 and component 2, respectively. The mobility coefficient λ is often taken as a constant λ_0 in the past, but is preferably a function of c in the following form:

$$\lambda = \lambda_0 c(1-c). \tag{2.36}$$

The Cahn–Hilliard equation with the volume fraction-dependent mobility is called singular or modified Cahn–Hilliard equation. If it is approximated simply by a constant value λ_0 in studying phase separated and immiscible fluids, the equation is the well-known Cahn–Hilliard equation. This hydrodynamic phase field is known as the quasi-incompressible model which was derived by two of the authors in [24]. It has also been derived by Shen

et al. [29] and Aki [4], respectively. The version in the mass fraction was given in [27]. This theory upholds the mass and momentum conservation laws while yielding a non-positive energy dissipation rate!

In the phase field model, the free energy density f can take on different forms depending on applications intended. In this paper, we consider the free energy density of the following form:

$$f(c, \nabla c) = k_B T \gamma \left(\frac{1}{2} \|\nabla c\|^2 + h(c) \right), \tag{2.37}$$

where T is the absolute temperature, k_B is the Boltzmann constant, γ is a parameter with the unit of a number density per unit length, which is in fact proportional to the product of the number density per unit volume and the square of the persistent length. The chemical potential is given by

$$\mu = k_B T \gamma \left(-\nabla^2 c + \frac{\mathrm{d}h}{\mathrm{d}c}(c) \right). \tag{2.38}$$

For the bulk potential $h(c)$, we consider the following two cases in this study.

Case 1: double-well free energy:

$$h(c) = \frac{1}{2\epsilon^2} c^2 (1-c)^2. \tag{2.39}$$

It is suitable for two immiscible fluids, where $\epsilon > 0$ is a small parameter characterizing the hydrophobic property between the two components.

Case 2: Flory–Huggins mixing free energy [12]:

$$h(c) = \frac{1}{\epsilon^2} \left(\frac{c}{N_1} ln(c) + \frac{1-c}{N_2} ln(1-c) + \chi c(1-c) \right), \tag{2.40}$$

where N_1 and N_2 are the polymerization index for component 1 and component 2, respectively, ϵ is a dimensionless parameter, and $\chi > 0$ is the mixing parameter.

2.3 Incompressible model (PFV)

If we use the volume-average velocity of the mixture $\mathbf{u} = c_1 \mathbf{v}_1 + c_2 \mathbf{v}_2$, the divergence free condition is satisfied automatically:

$$\nabla \cdot \mathbf{u} = \nabla \cdot (c_1 \mathbf{v}_1 + c_2 \mathbf{v}_2) = \nabla \cdot \left(\tfrac{\rho_1}{\hat{\rho}_1} \mathbf{v}_1 + \tfrac{\rho_2}{\hat{\rho}_2} \mathbf{v}_2 \right) = -\tfrac{\partial}{\partial t} \left(\tfrac{\rho_1}{\hat{\rho}_1} + \tfrac{\rho_2}{\hat{\rho}_2} \right) = -\tfrac{\partial}{\partial t} (c_1 + c_2) = 0. \tag{2.41}$$

We rewrite the mass conservation law for each component using the volume-average velocity as

$$\begin{aligned} \partial_t \rho_1 + \nabla \cdot (\rho_1 \mathbf{u} + \mathbf{J}_1) &= 0, \\ \partial_t \rho_2 + \nabla \cdot (\rho_2 \mathbf{u} + \mathbf{J}_2) &= 0, \end{aligned} \tag{2.42}$$

where $\mathbf{J}_1 = \rho_1(\mathbf{v}_1 - \mathbf{u})$, $\mathbf{J}_2 = \rho_2(\mathbf{v}_2 - \mathbf{u})$ are the fluxes related to $\mathbf{u}$. The total mass conservation is

$$\partial_t \rho + \nabla \cdot (\rho \mathbf{u} + \mathbf{J}_1 + \mathbf{J}_2) = 0. \tag{2.43}$$

Because $c_i = \frac{\rho_i}{\hat{\rho}_i}$, we have

$$\partial_t c_i + \nabla \cdot \left(c_i \mathbf{u} + \tfrac{\mathbf{J}_i}{\hat{\rho}_i} \right) = 0, \ i = 1, 2. \tag{2.44}$$

It is easy to find that $\frac{\mathbf{J}_1}{\hat{\rho}_1} + \frac{\mathbf{J}_2}{\hat{\rho}_2} = \frac{\rho_1(\mathbf{v}_1 - \mathbf{u})}{\hat{\rho}_1} + \frac{\rho_2(\mathbf{v}_2 - \mathbf{u})}{\hat{\rho}_2} = 0$. Then $\mathbf{J}_2 = -\frac{\hat{\rho}_2}{\hat{\rho}_1} \mathbf{J}_1$. As alluded earlier, we use $c = c_1$ and $\mathbf{J} = \mathbf{J}_1$, the equations for c, ρ are given, respectively, by

$$\begin{aligned} \partial_t c + \nabla \cdot \left(c \mathbf{u} + \tfrac{\mathbf{J}}{\hat{\rho}_1} \right) &= 0, \\ \partial_t \rho + \nabla \cdot \left(\rho \mathbf{u} + \left(1 - \tfrac{\hat{\rho}_2}{\hat{\rho}_1} \right) \mathbf{J} \right) &= 0. \end{aligned} \tag{2.45}$$

We remark that due to mass conservation, $\rho\mathbf{v} = \rho\mathbf{u} + (1 - \frac{\hat{\rho}_2}{\hat{\rho}_1})\mathbf{J}$. The two momenta can be very different when the density ratio is far from 1.

The balance of linear momentum states that

$$\partial_t(\rho\mathbf{v}) + \nabla\cdot(\rho\mathbf{v}\mathbf{v}) = \nabla\cdot\sigma + \mathbf{F}_e. \tag{2.46}$$

We substitute

$$\rho\mathbf{v} = \rho\mathbf{u} + \left(1 - \frac{\hat{\rho}_2}{\hat{\rho}_1}\right)\mathbf{J} \tag{2.47}$$

into the balance of linear momentum equation to obtain

$$\rho\left[\partial_t\left(\mathbf{u} + \frac{1}{\rho}\left(1 - \frac{\hat{\rho}_2}{\hat{\rho}_1}\right)\mathbf{J}\right) + \left(\mathbf{u} + \frac{1}{\rho}\left(1 - \frac{\hat{\rho}_2}{\hat{\rho}_1}\right)\mathbf{J}\right)\cdot\nabla\left(\mathbf{u} + \frac{1}{\rho}\left(1 - \frac{\hat{\rho}_2}{\hat{\rho}_1}\right)\mathbf{J}\right)\right] = \nabla\cdot\sigma + \mathbf{F}_e. \tag{2.48}$$

We drop $\partial_t(\frac{1}{\rho}(1 - \frac{\hat{\rho}_2}{\hat{\rho}_1})\mathbf{J})$, $(\frac{1}{\rho}(1 - \frac{\hat{\rho}_2}{\hat{\rho}_1})\mathbf{J})\cdot\nabla[\frac{1}{\rho}(1 - \frac{\hat{\rho}_2}{\hat{\rho}_1})\mathbf{J}]$ and $\mathbf{u}\cdot\nabla[\frac{1}{\rho}(1 - \frac{\hat{\rho}_2}{\hat{\rho}_1})\mathbf{J}]$ from the above linear momentum balance equation, to have the following transport equation of the volume-average velocity

$$\rho(\partial_t\mathbf{u} + \mathbf{u}\cdot\nabla\mathbf{u}) = \nabla\cdot\mathbf{S} - \nabla\Pi - \left(1 - \frac{\hat{\rho}_2}{\hat{\rho}_1}\right)\mathbf{J}\cdot\nabla\mathbf{u} + \mathbf{F}_e, \tag{2.49}$$

where $\sigma = \mathbf{S} - \Pi\mathbf{I}$, Π is the hydrostatic pressure, and $\mathbf{I}$ is the identity matrix. We introduce $\mathbf{T}$ as $\mathbf{T} = \mathbf{S} - \Pi\mathbf{I} - (1 - \frac{\hat{\rho}_2}{\hat{\rho}_1})\mathbf{u}\mathbf{J}$, the truncated pseudo linear momentum equation is written as

$$\partial_t(\rho\mathbf{u}) + \nabla\cdot(\rho\mathbf{u}\mathbf{u}) = \nabla\cdot\mathbf{T} + \mathbf{F}_e, \tag{2.50}$$

here mass conservation (2.43) is used. This equation is the original key assumption of the pseudo linear momentum equation in Abels et al.'s paper [3]. Here we have shown clearly the difference between the pseudo and real linear momentum equations. The pseudo linear momentum equation is an approximation to the real one by dropping three terms, which are related to the mass flux and proportional to the density difference. This balance equation is identical to the linear momentum balance equation only when the densities are equal. This deviation from the linear momentum balance portends the potential difference in dynamical predictions from the two models.

Following the previous practice formally, we define the free energy of the system as follows

$$E^{\text{total}} = \int_V \left(\frac{\rho}{2}\|\mathbf{u}\|^2\right)\mathrm{d}\mathbf{x} + F + G. \tag{2.51}$$

The kinetic energy density is represented by $\frac{\rho}{2}\|\mathbf{u}\|^2$, F is the bulk free energy, and G is the boundary free energy, as described in the previous subsection. Once again, we remark that $\frac{\rho}{2}\|\mathbf{u}\|^2$ is not the true kinetic energy and it's merely an approximation to the kinetic energy. So, the free energy of the system is an approximation to the true free energy of the system. This discrepancy is another source of difference in dynamical predictions from the two models. The energy dissipation rate at a constant absolute temperature T is given by

$$\frac{\mathrm{d}E^{\text{total}}}{\mathrm{d}t} = \int_V \mathrm{d}\mathbf{x}\left\{\frac{1}{2}\frac{\partial\left(\rho\|\mathbf{u}\|^2\right)}{\partial t} + \mu\frac{\partial c}{\partial t}\right\} + \int_{\partial V}\mathrm{d}S\left\{\mathbf{n}\cdot\frac{\partial f}{\partial(\nabla c)}\frac{\partial c}{\partial t} + \frac{\partial g}{\partial c}\frac{\partial c}{\partial t}\right\}. \tag{2.52}$$

We assume the following so that the surface integral is zero:

$$\left[\mathbf{n}\cdot\frac{\partial f}{\partial\nabla c} + \frac{\partial g}{\partial c}\right]|_{\partial V} = 0. \tag{2.53}$$

By using the transport equation of c, the conservations of the total mass, the pseudo linear momentum and $\nabla\cdot\mathbf{u} = 0$, we have

$$\begin{aligned}\frac{\mathrm{d}E^{\text{total}}}{\mathrm{d}t} &= \int_V \mathrm{d}\mathbf{x}\left\{\frac{1}{2}\|\mathbf{u}\|^2\partial_t\rho + \rho\mathbf{u}\cdot\partial_t\mathbf{u} + \mu\frac{\partial c}{\partial t}\right\}\\ &= \int_V \mathrm{d}\mathbf{x}\left\{-\frac{1}{2}\|\mathbf{u}\|^2\left(\nabla\cdot\left(\rho\mathbf{u} + \left(1 - \frac{\hat{\rho}_2}{\hat{\rho}_1}\right)\mathbf{J}\right)\right)\right.\end{aligned}$$

$$
\begin{aligned}
&+\mathbf{u}\cdot\left(-\rho\mathbf{u}\cdot\nabla\mathbf{u}+\nabla\cdot\mathbf{S}-\nabla\Pi-\left(1-\frac{\hat{\rho}_2}{\hat{\rho}_1}\right)\mathbf{J}\cdot\nabla\mathbf{u}+\mathbf{F}_e\right)-\mu\nabla\cdot\left(c\mathbf{u}+\frac{\mathbf{J}}{\hat{\rho}_1}\right)\Bigg\}\\
&=\int_V \mathrm{d}\mathbf{x}\left\{-\nabla\mathbf{u}:\mathbf{S}+\mathbf{u}\cdot(c\nabla\mu+\mathbf{F}_e)+\mathbf{J}\cdot\left(\frac{\nabla\mu}{\hat{\rho}_1}\right)\right\}\\
&\quad+\int_{\partial V}\mathrm{d}S\left\{\mathbf{u}\cdot\left(-\frac{1}{2}\rho\|\mathbf{u}\|^2\mathbf{I}-c\mu\mathbf{I}+\mathbf{S}\right)\cdot\mathbf{n}-\left(\frac{\mu}{\hat{\rho}_1}+\frac{1}{2}\left(1-\frac{\hat{\rho}_2}{\hat{\rho}_1}\right)\|\mathbf{u}\|^2\right)\mathbf{J}\cdot\mathbf{n}\right\}. \qquad (2.54)
\end{aligned}
$$

If we assume $\mathbf{u}=0$ and $\mathbf{J}\cdot\mathbf{n}=0$ at the boundary, the last surface integration is zero. These define additional boundary conditions for the velocity and the internal variable c via the excessive flux. We denote the strain rate tensor as

$$
\mathbf{D}=\frac{1}{2}\left(\nabla\mathbf{u}+\nabla\mathbf{u}^T\right). \qquad (2.55)
$$

Then, we define

$$
\mathbf{S}=2\eta\mathbf{D},\quad \mathbf{F}_e=-c\nabla\mu,\quad \mathbf{J}=-\lambda\hat{\rho}_1\nabla\mu, \qquad (2.56)
$$

where η is the shear viscosity coefficient and λ is the mobility coefficient. Finally, the energy dissipation rate is shown as non-positive,

$$
\frac{\mathrm{d}E^{\mathrm{total}}}{\mathrm{d}t}=-\int_V \mathrm{d}\mathbf{x}\left\{2\eta\mathbf{D}:\mathbf{D}+\lambda\|\nabla\mu\|^2\right\}\le 0. \qquad (2.57)
$$

It is different from (2.33) in that the energy dissipation rate is independent of the density ratio $\frac{\hat{\rho}_1}{\hat{\rho}_2}$ explicitly in this model.

We summarize the equations in the hydrodynamic phase field model with volume-average velocity, named PFV, in the following,

$$
\begin{aligned}
&\partial_t c+\mathbf{u}\cdot\nabla c=\nabla\cdot(\lambda\nabla\mu),\\
&\nabla\cdot\mathbf{u}=0,\\
&\rho=(\hat{\rho}_1-\hat{\rho}_2)c+\hat{\rho}_2,\\
&\rho\left(\tfrac{\partial\mathbf{u}}{\partial t}+\mathbf{u}\cdot\nabla\mathbf{u}\right)=-\nabla\Pi+2\nabla\cdot(\eta\mathbf{D})+\lambda(\hat{\rho}_1-\hat{\rho}_2)(\nabla\mu\cdot\nabla)\mathbf{u}-c\nabla\mu.
\end{aligned} \qquad (2.58)
$$

The viscosity coefficients for the fluid mixture are interpolated through the volume fraction and given by

$$
\eta=c\eta_1+(1-c)\eta_2, \qquad (2.59)
$$

where $\eta_{1,2}$ are constant shear viscosities for fluid component 1 and component 2, respectively. The mobility coefficient λ is preferably a function of c in the form $\lambda=\lambda_0 c(1-c)$, but often taken as a constant λ_0 for convenience in the past.

2.4 Non-dimensionalization

We use a characteristic timescale t_0 and length scale l_0 to non-dimensionalize the physical variables as follows:

$$
\tilde{t}=\tfrac{t}{t_0},\ \tilde{\mathbf{x}}=\tfrac{\mathbf{x}}{l_0},\ \tilde{\mathbf{v}}=\tfrac{\mathbf{v}t_0}{l_0},\ \tilde{\mathbf{u}}=\tfrac{\mathbf{u}t_0}{l_0},\ \tilde{\Pi}=\tfrac{\Pi t_0^2}{\hat{\rho}_2 l_0^2}.
$$

Then, the non-dimensionalized parameters are

$$
Re_i^s=\tfrac{\hat{\rho}_2 l_0}{\eta_i t_0},\ Re_i^v=\tfrac{\hat{\rho}_2 l_0}{\nu_i t_0},\ \Lambda=\tfrac{\lambda_0\gamma k_B T t_0}{l_0^4},\ \tilde{\epsilon}=\tfrac{\epsilon}{l_0},\ \tilde{\rho}=1-\left(1-\tfrac{\hat{\rho}_1}{\hat{\rho}_2}\right)c, \qquad (2.60)
$$

where Re_i^s and Re_i^v, $i=1,2$ denote the Reynolds numbers corresponding to the shear and volumetric stresses and Λ is the dimensionless mobility parameter. We also denote

$$
\tfrac{1}{Re^s}=\tfrac{c}{Re_1^s}+\tfrac{1-c}{Re_2^s},\quad \tfrac{1}{Re^v}=\tfrac{c}{Re_1^v}+\tfrac{1-c}{Re_2^v}, \qquad (2.61)
$$

where Re^s and Re^v are the effective Reynolds numbers of the mixture. First, we choose l_0 so that the dimensionless length in the x-direction of the fluid domain is $L_x = 1$. Then, we set the parameter group of the pressure Π in the dimensionless c-equation to be $\frac{\hat{\rho}_2 l_0^4}{\gamma k_B T t_0^2} = 1$ to select the timescale $t_0 = \sqrt{\frac{\hat{\rho}_2 l_0^4}{\gamma k_B T}}$. For simplicity, we drop the $\tilde{}$ on the dimensionless variables and the parameters. The total free energy is scaled by the characteristic energy $\hat{\rho}_2(\frac{l_0}{t_0})^2$, and the dimensionless total free energy is

$$E^{\text{total}} = \int_V \left(\frac{\rho}{2}\|\mathbf{v}\|^2 + \frac{1}{2}\|\nabla c\|^2 + h(c) \right) \mathrm{d}\mathbf{x}, \tag{2.62}$$

where $h(c) = \frac{1}{2\epsilon^2}c^2(1-c)^2$ for double-well energy or $\frac{1}{\epsilon^2}(\frac{c}{N_1}ln(c) + \frac{1-c}{N_2}ln(1-c) + \chi c(1-c))$ for Flory–Huggins energy, in PFM model. In PFV model, we replace $\mathbf{v}$ by $\mathbf{u}$ in (2.62). Here we set $g = 0$ to ignore the interfacial free energy. The corresponding boundary condition becomes $\mathbf{n} \cdot \frac{\partial f}{\partial \nabla c} = \mathbf{n} \cdot \nabla c = 0$, which is homogenous Neumann boundary condition for c.

The governing equations for the two phase field models in these dimensionless variables are then given by:

PFM model:

$$\begin{aligned} &\partial_t c + \nabla \cdot (c\mathbf{v}) = \nabla \cdot \left(\Lambda \nabla \left(\mu + \left(1 - \tfrac{\hat{\rho}_1}{\hat{\rho}_2} \right) \Pi \right) \right), \\ &\nabla \cdot \mathbf{v} = \left(1 - \tfrac{\hat{\rho}_1}{\hat{\rho}_2} \right) \nabla \cdot \left(\Lambda \nabla \left(\mu + \left(1 - \tfrac{\hat{\rho}_1}{\hat{\rho}_2} \right) \Pi \right) \right), \\ &\rho \left(\tfrac{\partial \mathbf{v}}{\partial t} + \mathbf{v} \cdot \nabla \mathbf{v} \right) = -\nabla \Pi + \nabla \cdot \left(\tfrac{1}{Re^s} \nabla \mathbf{v} \right) + \nabla \left(\left(\tfrac{1}{Re^s} + \tfrac{1}{Re^v} \right) \nabla \cdot \mathbf{v} \right) - c \nabla \mu. \end{aligned} \tag{2.63}$$

PFV model:

$$\begin{aligned} &\partial_t c + \mathbf{u} \cdot \nabla c = \nabla \cdot (\Lambda \nabla \mu), \quad \nabla \cdot \mathbf{u} = 0, \\ &\rho \left(\tfrac{\partial \mathbf{u}}{\partial t} + \mathbf{u} \cdot \nabla \mathbf{u} \right) = -\nabla \Pi + \nabla \cdot \left(\tfrac{1}{Re^s} \nabla \mathbf{u} \right) - \Lambda \left(1 - \tfrac{\hat{\rho}_1}{\hat{\rho}_2} \right) (\nabla \mu \cdot \nabla) \mathbf{u} - c \nabla \mu. \end{aligned} \tag{2.64}$$

Here $\rho = 1 - (1 - \frac{\hat{\rho}_1}{\hat{\rho}_2})c$. And the chemical potential of the free energy is

$$\mu = -\nabla^2 c + h^{(1)}(c). \tag{2.65}$$

For the double-well free energy,

$$h^{(1)}(c) = \tfrac{1}{\epsilon^2} c(1-c)(1-2c). \tag{2.66}$$

For the Flory–Huggins mixing energy, with $N_1 = 1$, $N_2 = 2$, $\chi = 2$ (the numerical values that we fix in this study),

$$h^{(1)}(c) = \tfrac{1}{\epsilon^2} \left(\ln c - \tfrac{1}{2} \ln(1-c) - 4c \right) + \text{constant}. \tag{2.67}$$

3 Theoretical comparison

In the derivation of the PFM model, we enforce the mass and momentum conservation although the transport equation of the volume fraction of one component uses a constitutive relation. In contrast, only the mass conservation is enforced in the derivation of the PFV model, where the transport equation for one component is obtained via a constitutive equation and the linear momentum equation is approximated. So strictly speaking, the momentum is not conserved in the PFV model. Moreover, the kinetic energy used in the PFV model is not exactly the true kinetic energy when the volume-average velocity is used. If we hypothetically assume the constitutive relation is exact, the PFV model only respects the mass conservation while the PFM model respects both the mass and the linear momentum conservation. In this regard, we tend to believe the PFM model is closer to the physical reality.

In addition to the above qualitative differences, the other obvious differences between the two models include that, in the PFM model, the velocity field is not divergence free and the hydrostatic pressure is coupled to the transport equation of the phase variable. Here, we want to expose another hidden difference in the

mobility coefficient between the two models, by explicitly expressing the transport equation of c_2, the volume fraction of fluid component 2 with $c_2 = 1 - c$.

The free energy density $f = f(c, \nabla c) = f(1 - c_2, -\nabla c_2)$. The chemical potential of c_2 is

$$\mu_2 = \frac{\partial f}{\partial c_2} - \nabla \cdot \frac{\partial f}{\partial(\nabla c_2)} = -\frac{\partial f}{\partial c} + \nabla \cdot \frac{\partial f}{\partial(\nabla c)} = -\mu. \tag{3.1}$$

Substituting the relations $c = 1 - c_2$ and $\mu = -\mu_2$ into the governing equations of the PFM model, and redefining the pressure as $\Pi_2 = \Pi - \mu_2$, then the momentum equation exhibits the same form as before

$$\rho\left(\frac{\partial \mathbf{v}}{\partial t} + \mathbf{v} \cdot \nabla \mathbf{v}\right) = -\nabla \Pi_2 + \nabla \cdot \left(\frac{1}{Re^s} \nabla \mathbf{v}\right) + \nabla\left(\left(\frac{1}{Re^s} + \frac{1}{Re^v}\right) \nabla \cdot \mathbf{v}\right) - c_2 \nabla \mu_2.$$

The equations of c and continuity equation $\nabla \cdot \mathbf{v}$ can be rewritten using c_2, μ_2, Π_2 as follows

$$\begin{aligned} \partial_t c_2 + \nabla \cdot (c_2 \mathbf{v}) &= \nabla \cdot \left(\Lambda_2 \nabla \left(\mu_2 + \left(1 - \frac{\hat{\rho}_2}{\hat{\rho}_1}\right) \Pi_2\right)\right), \\ \nabla \cdot \mathbf{v} &= \left(1 - \frac{\hat{\rho}_2}{\hat{\rho}_1}\right) \nabla \cdot \left(\Lambda_2 \nabla \left(\mu_2 + \left(1 - \frac{\hat{\rho}_2}{\hat{\rho}_1}\right) \Pi_2\right)\right), \end{aligned} \tag{3.2}$$

where the density ratio is $\frac{\hat{\rho}_2}{\hat{\rho}_1}$, the inverse of $\frac{\hat{\rho}_1}{\hat{\rho}_2}$, and the mobility Λ_2 of c_2 is

$$\Lambda_2 = \Lambda \left(\frac{\hat{\rho}_1}{\hat{\rho}_2}\right)^2. \tag{3.3}$$

This shows that the "formal" mobility coefficients of the volume fractions of the fluid components differ in the PFM model. In the transport equation for the volume fraction of the second fluid component, the dependence of mobility on the density ratio is explicit if the mobility coefficient for the first fluid component is given, exposing the role of density differentiation in the transport process and a hidden asymmetry in the form of the transport equation for the volume fractions in the PFM model. Since $c + c_2 = 1$, dynamics of both volume fractions is supposed to be the same. But their transport equations look different. It indicates that the pressure in the quasi-incompressible model must play an important role in the transport of the phase variables than a normal hydrostatic pressure does in an incompressible model.

In contrast, we rewrite the governing system of equations using the volume fraction of the other component in the PFV model, the governing equations are given by

$$\begin{aligned} &\partial_t c_2 + \mathbf{u} \cdot \nabla c_2 = \nabla \cdot (\Lambda \nabla \mu_2), \quad \nabla \cdot \mathbf{u} = 0, \\ &\rho\left(\frac{\partial \mathbf{u}}{\partial t} + \mathbf{u} \cdot \nabla \mathbf{u}\right) = -\nabla \hat{\Pi} + \nabla \cdot \left(\frac{1}{Re^s} \nabla \mathbf{u}\right) - \Lambda\left(\frac{\hat{\rho}_1}{\hat{\rho}_2} - 1\right)(\nabla \mu_2 \cdot \nabla)\mathbf{u} - c_2 \nabla \mu_2, \end{aligned} \tag{3.4}$$

where the new pressure is $\hat{\Pi} = \Pi - \mu_2$. In the new momentum equation, the forcing term $-\Lambda(1 - \frac{\hat{\rho}_1}{\hat{\rho}_2})(\nabla \mu \cdot \nabla)\mathbf{u}$ changes to $-\Lambda(\frac{\hat{\rho}_1}{\hat{\rho}_2} - 1)(\nabla \mu_2 \cdot \nabla)\mathbf{u}$. The mobility for transporting c_2 is also Λ, independent of the density ratio $\frac{\hat{\rho}_1}{\hat{\rho}_2}$. So, the transport equations of both volume fractions are identical in form. This is the most important departure from the PFM model.

The second major difference lies in the energy dissipation rates of the two models. The energy dissipation rate in the PFM model depends on the density ratio explicitly, while that in the PFV model does implicitly only through the volume-average velocity. Further discrepancies between the two models and detailed comparisons will be discussed in the next two sections via a linear stability analysis and numerical simulations on nonlinear dynamics.

4 Linear stability analysis

In this section, we examine linear stability prediction from the two models to further expose their differences. We consider the solution of the governing equations which are only varying in the x direction and homogenous in the other two directions. That means the unknown variables are functions of time t and one spatial variable $x \in R^1$, where the characteristic length scale l_0 is chosen as a typical length in which the fluid phenomenon is observed. The equations of the two models in 1D space are listed below:

PFM model:

$$\begin{aligned}
&\partial_t c + (c\mathbf{v}_1)' = \left(\Lambda\left(\mu + \left(1-\tfrac{\hat{\rho}_1}{\hat{\rho}_2}\right)\Pi\right)'\right)',\\
&\mathbf{v}_1' = \left(1-\tfrac{\hat{\rho}_1}{\hat{\rho}_2}\right)\left(\Lambda\left(\mu + \left(1-\tfrac{\hat{\rho}_1}{\hat{\rho}_2}\right)\Pi\right)'\right)',\\
&\rho\tfrac{\partial \mathbf{v}_1}{\partial t} = -\rho\mathbf{v}_1\mathbf{v}_1' - \Pi' + \left(\tfrac{1}{Re^s}\mathbf{v}_1'\right)' + \left(\left(\tfrac{1}{Re^s}+\tfrac{1}{Re^v}\right)\mathbf{v}_1'\right)' - c\mu\,',\\
&\rho\tfrac{\partial \mathbf{v}_2}{\partial t} = -\rho\mathbf{v}_1\mathbf{v}_2' + \left(\tfrac{1}{Re^s}\mathbf{v}_2'\right)', \quad \rho\tfrac{\partial \mathbf{v}_3}{\partial t} = -\rho\mathbf{v}_1\mathbf{v}_3' + \left(\tfrac{1}{Re^s}\mathbf{v}_3'\right)'.
\end{aligned} \tag{4.1}$$

Here $(\cdot)' = \frac{\partial(\cdot)}{\partial x}$ and $\mathbf{v} = (\mathbf{v}_1, \mathbf{v}_2, \mathbf{v}_3)$. The pressure Π can be solved from the second equation:

$$\Pi' = \tfrac{\mathbf{v}_1}{\beta^2\Lambda} - \tfrac{\mu\,'}{\beta}, \tag{4.2}$$

where $\beta = 1 - \frac{\hat{\rho}_1}{\hat{\rho}_2}$, $\mathbf{v}_2$ and $\mathbf{v}_3$ decouple from the rest of the equations. Then, the equations reduce to a system of coupled equations for $(c, \mathbf{v}_1)$,

$$\begin{aligned}
&\partial_t c + (c\mathbf{v}_1)' = \tfrac{\mathbf{v}_1'}{\beta},\\
&\rho\tfrac{\partial \mathbf{v}_1}{\partial t} = -\rho\mathbf{v}_1\mathbf{v}_1' + \left(\tfrac{1}{Re^s}\mathbf{v}_1'\right)' + \left(\left(\tfrac{1}{Re^s}+\tfrac{1}{Re^v}\right)\mathbf{v}_1'\right)' - \tfrac{\mathbf{v}_1}{\beta^2\Lambda} + \left(\tfrac{1}{\beta} - c\right)\mu\,'.
\end{aligned} \tag{4.3}$$

PFV model:

$$\begin{aligned}
&\partial_t c + \mathbf{u}_1 c' = (\Lambda\mu\,')', \quad \mathbf{u}_1' = 0,\\
&\rho\tfrac{\partial \mathbf{u}_1}{\partial t} = -\Pi' + \left(\tfrac{1}{Re^s}\mathbf{u}_1'\right)' - \Lambda\left(1-\tfrac{\hat{\rho}_1}{\hat{\rho}_2}\right)\mu\,'\mathbf{u}_1' - c\mu\,',\\
&\rho\tfrac{\partial \mathbf{u}_2}{\partial t} = \left(\tfrac{1}{Re^s}\mathbf{u}_2'\right)' - \Lambda\left(1-\tfrac{\hat{\rho}_1}{\hat{\rho}_2}\right)\mu\,'\mathbf{u}_2',\\
&\rho\tfrac{\partial \mathbf{u}_3}{\partial t} = \left(\tfrac{1}{Re^s}\mathbf{u}_3'\right)' - \Lambda\left(1-\tfrac{\hat{\rho}_1}{\hat{\rho}_2}\right)\mu\,'\mathbf{u}_3'.
\end{aligned} \tag{4.4}$$

Here $\mathbf{u} = (\mathbf{u}_1, \mathbf{u}_2, \mathbf{u}_3)$. Firstly, we observe that $\mathbf{u}_1 = const = 0$ due to the diverge free and boundary conditions at infinity. Then, all equations decouple so that the equation of c can be solved independently

$$\partial_t c = (\Lambda\mu\,')'. \tag{4.5}$$

The pressure is given by the solution of the equation $\Pi' = -c\mu\,'$, and $\mathbf{u}_2, \mathbf{u}_3$ can be solved from their own equations. For the two models, the chemical potential is $\mu = h^{(1)}(c) - (c')'$.

We notice that both models admit a constant solution:

$$c = c_0, \quad \mathbf{v}_1 = 0 (\mathbf{u}_1 = 0), \quad \Pi = 0, \tag{4.6}$$

where c_0 is constant and $c_0 \in [0, 1]$. We next study linear stability of the constant steady state subject to periodic boundary conditions with respect to the two models.

We perturb constant solution (4.6) as follows:

$$c = c_0 + \delta e^{\alpha t + ik\cdot x} c_1^1, \quad \mathbf{v}_1 = \delta e^{\alpha t + ik\cdot x}\mathbf{v}_1^1 \left(\mathbf{u}_1 = \delta e^{\alpha t + ik\cdot x}\mathbf{u}_1^1\right), \quad \Pi = \delta e^{\alpha t + ik\cdot x}\Pi_1, \tag{4.7}$$

where $\delta \ll 1$ is a small perturbation, c_1^1, $\mathbf{v}_1^1(\mathbf{u}_1^1)$, Π_1 are constants. For the PFM model, by truncating at the linear order of δ, we write the governing system of equations for the perturbations into a matrix form,

$$\begin{pmatrix} \alpha & \left(c_0 - \frac{1}{\beta}\right) ik \\ -ik\left(c_0 - \frac{1}{\beta}\right)\left(k^2 + h^{(2)}(c_0)\right) & (1-\beta c_0)\alpha + \left(\frac{2}{Re_0^s} + \frac{1}{Re_0^v}\right)k^2 + \frac{1}{\Lambda\beta^2} \end{pmatrix} \begin{pmatrix} c_1^1 \\ \mathbf{v}_1^1 \end{pmatrix} = 0, \tag{4.8}$$

where $h^{(2)}(c_0) = \frac{1}{\epsilon^2}(1-6c_0+6c_0^2)$ for the double-well potential or $h^{(2)}(c_0) = \frac{1}{\epsilon^2}(\frac{1}{c_0} + \frac{1}{2(1-c_0)} - 4)$ for the Flory–Huggins potential, and the Reynolds numbers Re_0^s, Re_0^v are given by $\frac{1}{Re_0^s} = \frac{c_0}{Re_1^s} + \frac{1-c_0}{Re_2^s}$, $\frac{1}{Re_0^v} = \frac{c_0}{Re_1^v} + \frac{1-c_0}{Re_2^v}$. The characteristic equation of the coefficient matrix is

$$(1-\beta c_0)\alpha^2 + \left[\left(\tfrac{2}{Re_0^s} + \tfrac{1}{Re_0^v}\right)k^2 + \tfrac{1}{\Lambda\beta^2}\right]\alpha + \left(c_0 - \tfrac{1}{\beta}\right)^2 k^2\left[k^2 + h^{(2)}(c_0)\right] = 0. \tag{4.9}$$

Because $\beta = 1 - \frac{\hat{\rho}_1}{\hat{\rho}_2} < 1$ and $c_0 \in [0, 1]$, then $1 - \beta c_0 > 0$. The unstable condition is

$$h^{(2)}(c_0) < 0. \tag{4.10}$$

The unstable wave number region is $0 < |k| < \sqrt{-h^{(2)}(c_0)}$, in which the positive growth rate is given by

$$\alpha_1 = \frac{-2(1-\beta c_0)^2 \Lambda k^2 \left[k^2 + h^{(2)}(c_0)\right]}{\left[1 + \Lambda\beta^2\left(\frac{2}{Re_0^s} + \frac{1}{Re_0^v}\right)k^2\right] + \sqrt{\left[1 + \Lambda\beta^2\left(\frac{2}{Re_0^s} + \frac{1}{Re_0^v}\right)k^2\right]^2 - 4\Lambda^2\beta^2(1-\beta c_0)^3 k^2\left[k^2 + h^{(2)}(c_0)\right]}}. \tag{4.11}$$

For the PFV model, the unstable condition is also (4.10) and in the unstable wave number region the positive growth rate is

$$\alpha_2 = -\Lambda k^2 \left[k^2 + h^{(2)}(c_0)\right]. \tag{4.12}$$

We remark that this unstable growth rate of the PFV model is independent of the density ratio!

When $\beta = 0$, i.e., $\hat{\rho}_1 = \hat{\rho}_2$, we have $\alpha_1 = \alpha_2$. In this case the two models are identical. When $0 < \beta < 1$, that is $\hat{\rho}_1 < \hat{\rho}_2$, it is easy to find that

$$\alpha_1 < -(1 - \beta c_0)^2 \Lambda k^2 \left[k^2 + h^{(2)}(c_0)\right] < \alpha_2. \tag{4.13}$$

It is consistent to the numerical result that when $\hat{\rho}_1 < \hat{\rho}_2$, the dynamic process of the PFM model is slower than that of the PFV model.

In the region $\beta < 0$, an analytic comparison of $\alpha_{1,2}$ is not feasible. We plot the growth rate as a function of (β, k) numerically. The parameter values used are listed in Table 1. We choose $c_0 = 0.4$, then the unstable wave number region is $|k| < \sqrt{1100} \approx 33.17$. In Fig. 3, the (β, k) space plotted is $[-10, 1] \times [0, 33]$. In this region, α_1 and α_2 are all positive. When β is not far from zero, $\alpha_1 > \alpha_2$ in the whole unstable wave number region; but when $|\beta|$ is large, $\alpha_1 > \alpha_2$ in small wave number region and $\alpha_1 < \alpha_2$ in the large wave number

Table 1 List of parameter values

Parameter	Re_1^s	Re_2^s	Re_1^v	Re_2^v	$\frac{\hat{\rho}_1}{\hat{\rho}_2}$	β	ϵ	Λ
Value	1	$10 \times Re_1^s$	$\frac{1}{4.3}$	$10 \times Re_1^v$	$0.99 \sim 10$	$1 - \frac{\hat{\rho}_1}{\hat{\rho}_2}$	0.02	5×10^{-6}

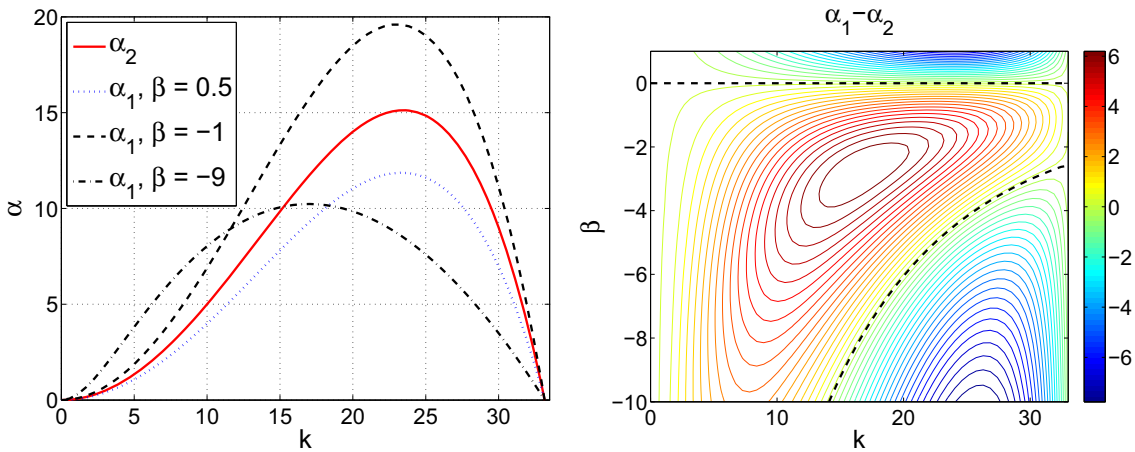

(a) Growth rates α_1, α_2 **(b)** Contour map of growth rate difference $\alpha_1 - \alpha_2$

Fig. 3 **a** Positive growth rates α_1, α_2 with three different values of β as functions of the wave number k. α_1 is the growth rate of the PFM model while α_2 is the growth rate of the PFV model. **b** The growth rate difference $\alpha_1 - \alpha_2$ in the (β, k) space. In the contour map (b), the black dashed curve is the zero level contour ($\alpha_1 - \alpha_2 = 0$). When $0 < \beta < 1$, $\alpha_1 < \alpha_2$. When $\beta < 0$, there are two cases: β not far from zero, $\alpha_1 > \alpha_2$; $|\beta|$ is large, $\alpha_1 > \alpha_2$ in small wave number region and $\alpha_1 < \alpha_2$ in the large wave number region. Heuristically, a larger growth rate indicates faster dynamics in the system

region. An asymptotic analysis can be used here when the mobility $\Lambda \ll 1$. If Λ is very small, and $|\beta k|$ is not large, we have

$$\alpha_1 \approx -(1-\beta c_0)^2 \Lambda k^2 \left[k^2 + h^{(2)}(c_0)\right] > \alpha_2. \tag{4.14}$$

It is consistent with the numerical studies in the next section. The dynamic process of the PFM model is faster than that of the PFV model when $\alpha_1 > \alpha_2$ and slower otherwise. The linear stability analysis indicates that growth dynamics in the PFM model depends on the density ratio while it does not in the PFV model.

5 Nonlinear dynamic simulations

One of the applications of phase field models is the study of coarsening dynamics or coalescent dynamics of single phase regions, represented by protuberances in the volume fraction function in a biphasic setting. We investigate coalescent dynamics of protuberances in biphasic systems using the two distinct models, focusing on comparing model predictions dynamically. The numerical scheme we use to solve the equations in the two models is the modified pressure-corrected projection scheme presented in paper [29], which is implemented in 1D space and time. The spatial 1D domain is $I = [0, 1]$. The boundary conditions are given as follows

$$c'|_{x=0,1} = 0,\ \mu'|_{x=0,1} = 0,\ \mathbf{v}_1|_{x=0,1} = 0. \tag{5.1}$$

The parameter values used in the study are listed in Table 1.

In the following numerical examples, the ratio of the two fluid densities $\frac{\hat{\rho}_1}{\hat{\rho}_2}$ is varied from 10 to 0.99 so that β varies from -9 to 0.01. We conduct the dynamical study using the double-well and the Flory–Huggins free energy with respect to a given initial condition of c as well as a random initial profile of c, respectively.

Before we present the numerical solutions, we first examine the long time behavior of the 1D systems. With this set of boundary conditions, we first solve for the steady states of the two models. For the PFV model, the steady states are governed by

$$\mathbf{u}_1 = 0, \quad \mu' = 0. \tag{5.2}$$

We then solve the transport equation of c in steady state in the PFM model and find $\mathbf{v}_1 = 0$, and the steady state of the volume fraction is governed by

$$\mu' = 0. \tag{5.3}$$

This indicates that the two models share the same 1-D steady states, governed by the critical points of the chemical potential. Thus, if there are any differences in these two models in their 1D prediction subject to the given boundary conditions, they show up in their respective transient dynamics.

5.1 Protuberance coalescence subject to a double-well potential

We first look at the protuberance coalescence subject to a double-well potential using the two hydrodynamic models. The initial conditions are given as follows

$$\begin{aligned} &\mathbf{v}_1(x,0) = 0, \quad \Pi(x,0) = 0, \\ &c(x,0) = \begin{cases} \tanh(2), & r_1 \le 0.1-a \text{ or } r_2 \le 0.1-a \\ \tanh((0.1+a-r_1)/a), & 0.1-a < r_1 < 0.1+a \\ \tanh((0.1+a-r_2)/a), & 0.1-a < r_2 < 0.1+a \\ 0, & \text{else}, \end{cases} \end{aligned} \tag{5.4}$$

where $r_1 = |x-0.35|$, $r_2 = |x-0.65|$ and $a = 0.05$. In the initial state of c, there are two protuberances next to each other in the middle of the domain, which finally coalesce into a large one at the end of our numerical simulations. First, we set the density ratio $\frac{\hat{\rho}_1}{\hat{\rho}_2} = 0.9$, i.e., $\beta = 0.1$. As shown in Fig. 4, the coalescent processes predicted using the two models are slightly different, the coalescent process in the PFM model is slower than that in the PFV model. In the second and third subfigure in Fig. 4, at time $t = 2, 4$, the volume fraction c near the middle point $x = 0.5$ in the PFM model is obviously smaller than that in the PFV model. In Fig. 4g, the curves of velocity $\mathbf{v}_1$ in PFM model are plotted, $\mathbf{v}_1$ is nonzero in the coalescent process, which is very different

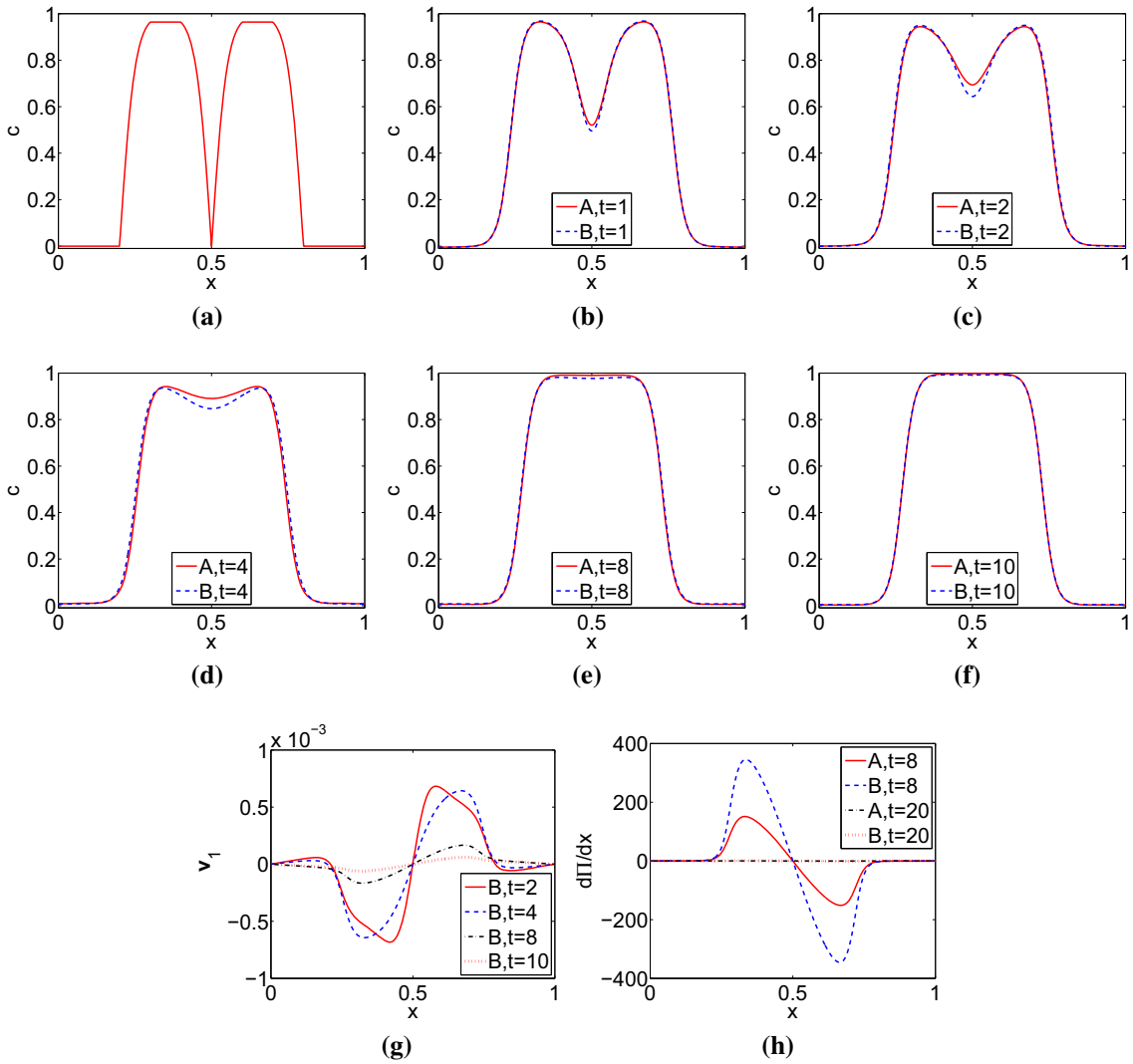

Fig. 4 Comparison of time-dependent protuberance coalescence dynamics. A: PFV model; B: PFM model. The first subfigure shows the initial state of c, where two protuberances are next to each other in the middle of the domain. The parameter value $\beta = 0.1$. When the difference of the two specific densities is large, the coalescent dynamic processes of the two models show some differences in time, the coalescent process of the PFM model is slower than that of the PFV model. But the final quasi-steady states are the same since the velocity and the gradients of pressure are all damped to zero at the end of the simulation, as shown in **g** and **h**

from zero velocity $\mathbf{u}_1 = 0$ in the PFM model. In Fig. 4h, however, the gradients of pressure of the two models are almost zero at time $t = 20$ and the final quasi-steady states are the same.

To study the role of the density ratio in coalescent dynamics, we further increase the density ratio to $\frac{\hat{\rho}_1}{\hat{\rho}_2} = 0.5$, i.e., $\beta = 0.5$. The difference of the two simulated dynamic processes becomes more prominent, shown in Fig. 5. For the PFV model, c reaches the quasi-steady state at about $t = 10$; but for the PFM model, c reaches the quasi-steady state at about $t = 40$. Velocity $\mathbf{v}_1$ in PFM model is also nonzero during the coalescent process. A more extreme example is given in Fig. 6, where the density ratio is $\frac{\hat{\rho}_1}{\hat{\rho}_2} = 0.1$ and $\beta = 0.9$. The coalescent dynamic process of the PFM model slows down significantly, where c reaches the quasi-steady state beyond $t = 350$. As we have shown in the above section, for the PFM model, the mobility of c_2 is $\Lambda_2 = \Lambda(\frac{\hat{\rho}_1}{\hat{\rho}_2})^2$. When $\frac{\hat{\rho}_1}{\hat{\rho}_2}$ is small, the mobility Λ_2 is small, so the dynamic process in the PFM model slows down. Physically, when the surrounding fluid matrix is heavier than the one in the protuberances, the coalescent dynamics tends to slow down as predicted by the PFM model.

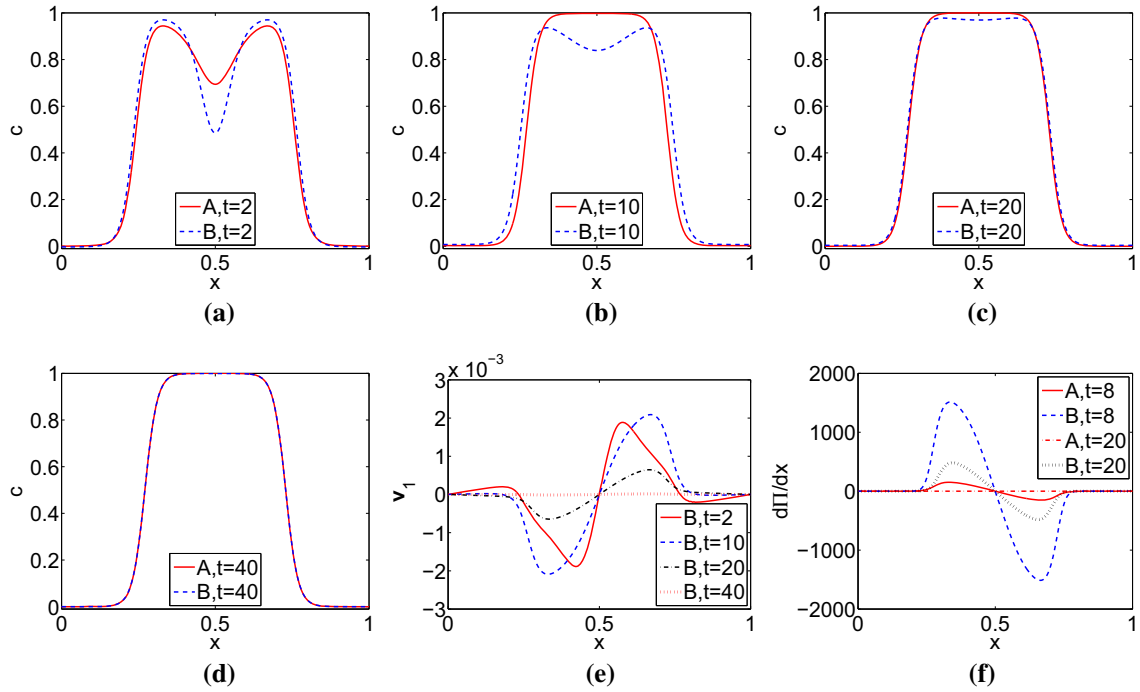

Fig. 5 Comparison of time-dependent protuberance coalescence dynamics. A: PFV model; B: PFM model. $\frac{\hat{\rho}_1}{\hat{\rho}_2} = 0.5$, $\beta = 0.5$. In comparison, when the difference of the two specific densities is larger, the coalescent dynamics of the PFM model is slower

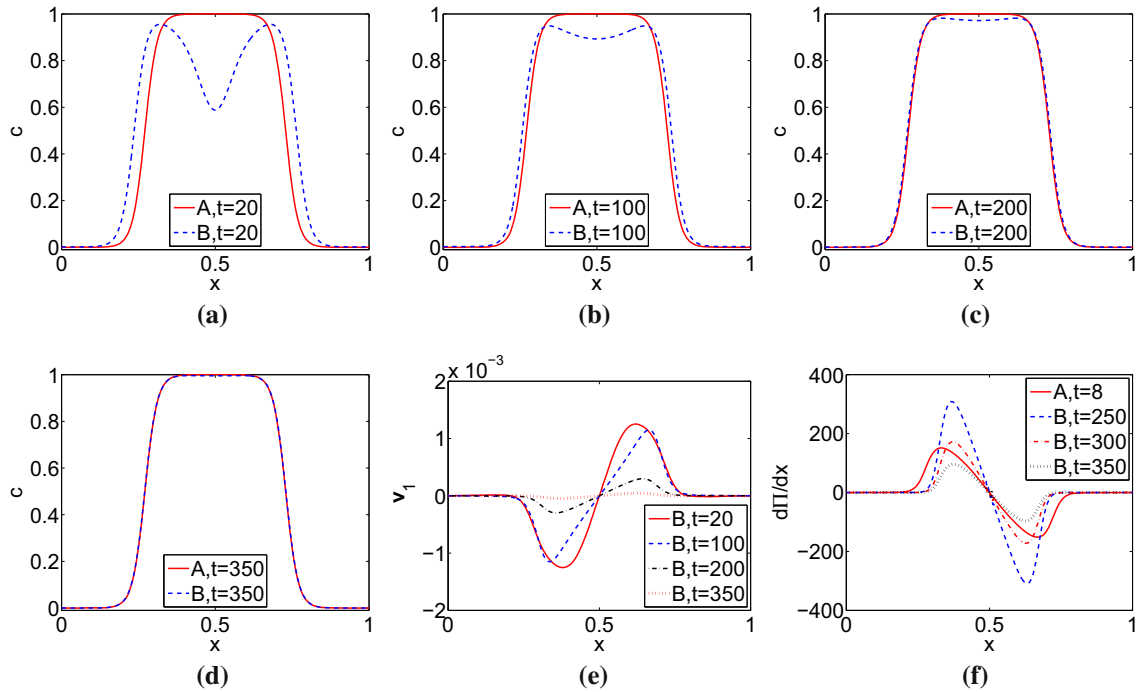

Fig. 6 Comparison of time-dependent protuberance coalescence dynamics. A: PFV model; B: PFM model. $\frac{\hat{\rho}_1}{\hat{\rho}_2} = 0.1$, $\beta = 0.9$. In the PFV model, c reaches the quasi-steady state at $t = 10$; but in the PFM model, it reaches it after $t = 350$. The dynamics predicted by the PFM model is much slower than that by the PFV model when the density ratio is small or β is close to 1. The pressure field predicted by the PFM model at $t = 350$ is still not uniform although the phases predicted by the two models match very well already

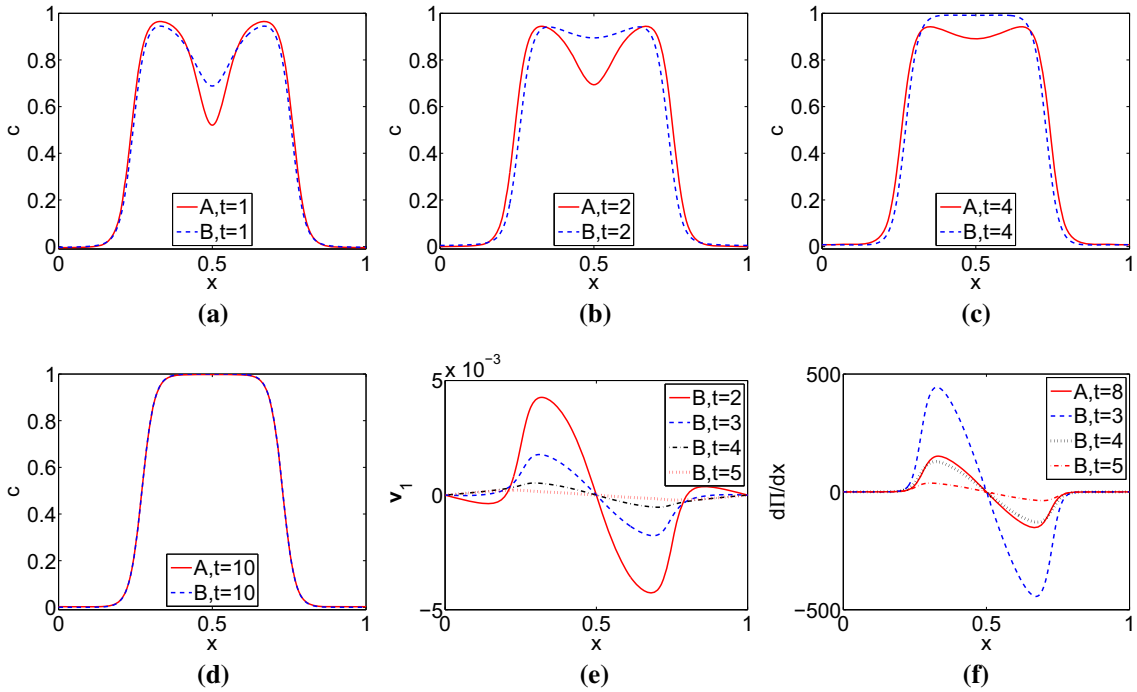

Fig. 7 Comparison of time-dependent protuberance coalescence dynamics. A: PFV model; B: PFM model. $\beta = -0.5$ and $\frac{\hat{\rho}_1}{\hat{\rho}_2} = 1.5$. In the PFV model, c reaches the quasi-steady state after time $t = 10$; but in the PFM model, it does it at time $t = 5$. The coalescent process of the PFM model is faster in this case

We next study the case where $\hat{\rho}_1 > \hat{\rho}_2$, i.e., β is negative. In Fig. 7, $\beta = -0.5$. The coalescent process of the PFM model is faster than that of the PFV model. This is because $\Lambda_2 = \Lambda(\frac{\hat{\rho}_1}{\hat{\rho}_2})^2$ is larger than Λ. In Fig. 8, the solutions of PFM model with different negative β values are shown at different time. The dynamic process becomes faster as β decreases ($|\beta|$ increases). This finding is consistent with the linear stability analysis in the long wave region, where the growth rate of the unstable mode in the PFM model α_1 increases with respect to $-\beta$. In this case, the heavier protuberances tend to merge faster when the ambient fluid matrix is lighter as predicted by the PFM model. In contrast, the PFV model does not discern the difference at all.

We plot the total energy with respect to a few selected values of β in Fig. 9. As we point out in the second section, the energy dissipation rate of PFM model (2.33) depends on the density ratio $\frac{\hat{\rho}_1}{\hat{\rho}_2}$ explicitly, but the energy dissipation rate of PFV model (2.57) does not explicitly. The energy plots in the numerical examples resonate with the observation. The total energy plots of all the cases converge to 33.3 eventually in the quasi-steady state. It is easy to understand this, because the final quasi-steady states of the two cases are the same. The transient states during the coalescent dynamic processes are quite different though. This figure shows that the energy decay process becomes faster as β decreases. It is consistent with the protuberance coalescent dynamic process of the fluid mixture alluded to earlier.

So far, the numerical examples have demonstrated the difference in transient dynamics between the predictions made by the two phase field models. We would like to see whether the difference only lies in the rate of coarsening (coalescent) dynamics, parametrized by the mobility coefficient. In another word, can we adjust the mobility parameter in one model to match the dynamics in the other? For this purpose, we fix $\beta = 0.5$ in the PFM model and $\Lambda = 5 \times 10^{-6}$ in the PFV model, then modify the mobility coefficient in the PFM model to be 3.1Λ, then, the energy curves of the two models match very well as shown in Fig. 10. The transient states of volume fraction c match well at different times as well. However, the gradients of pressure do not match so well at different times, but the relative difference is not huge either. This shows that by adjusting the rate of dynamics in one model, we may be able to match the transient dynamics to the other model to some extent. This matching game is attainable for the double-well potential at least for the examples we examined, but it is hardly feasible for the Flory–Huggins potential as we will show below, where the transient dynamics is more complex.

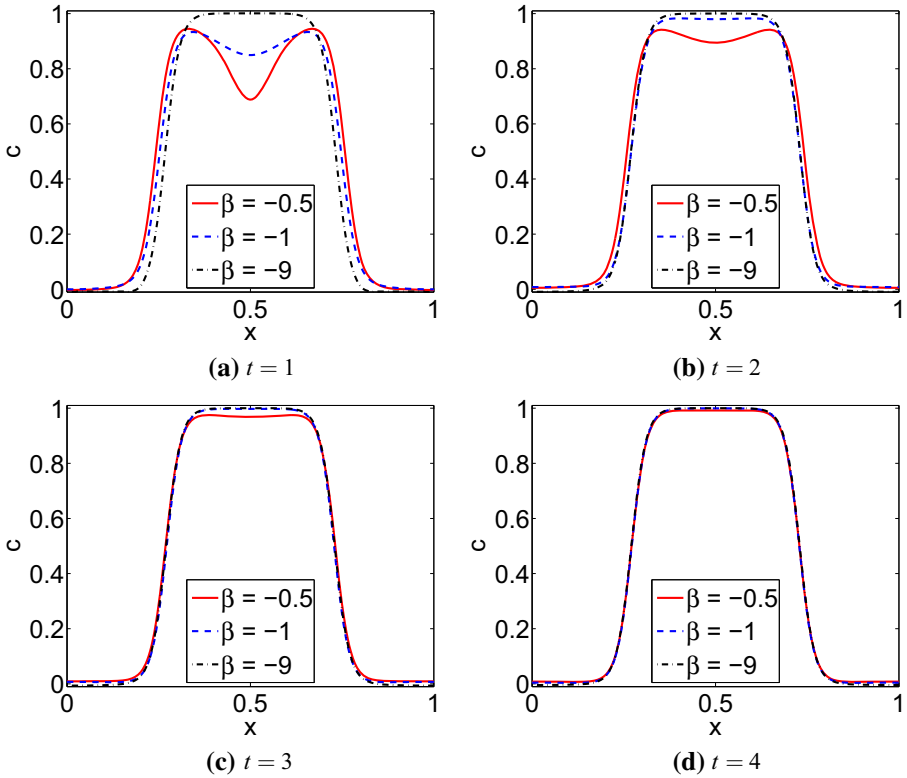

Fig. 8 Solutions of the PFM model with negative $\beta = -0.5, -1, -9$ at different times. **a** When $\beta = -9$, the solution is near quasi-steady at $t = 1$; **b** and **c** when $\beta = -1, -9$, the solutions are near quasi-steady at $t = 2, 3$, respectively; **d** when $\beta = -0.5, -1, -9$, the solutions are near quasi-steady at $t = 4$. This simulation shows that coarsening dynamics becomes faster as β decreases

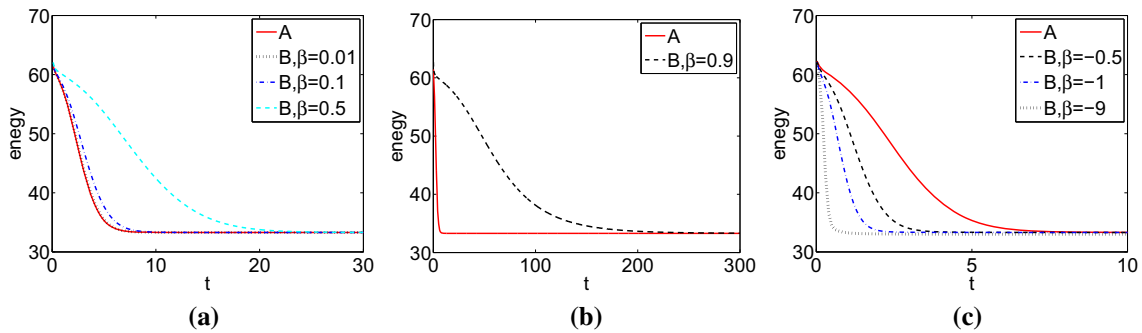

Fig. 9 Comparison of total energy curves. A: PFV model; B: PFM model. The rate of the energy decay decreases with respect to β. This behavior is consistent with growth dynamics of the PFM model in the long wave region in the linear stability analysis

5.2 Coalescent dynamics with the Flory–Huggins free energy

In this numerical example, we consider the Flory–Huggins free energy. The initial conditions are given by

$$\mathbf{v}_1(x, 0) = 0, \quad \Pi(x, 0) = 0, \quad c(x, 0) = 0.5 + 0.2\,\mathrm{Rand}(0, 1), \tag{5.5}$$

where Rand(0, 1) is the random number generator subject to the standard uniform distribution in the open interval (0, 1); then, $c(x, 0) \in (0.3, 0.7)$. We first generate the random numbers and save them; then, the other numerical simulations are all based on the same initial state except that the parameter β is allowed to vary. In Fig. 11, we use $\beta = 0.1$ and in Fig. 12, $\beta = 0.5$. In each example, we find that the coalescent process of the PFM model is slower than that of the PFV model as expected. The final quasi-steady states are the same between the two models even with different values of parameter β when using the same initial state.

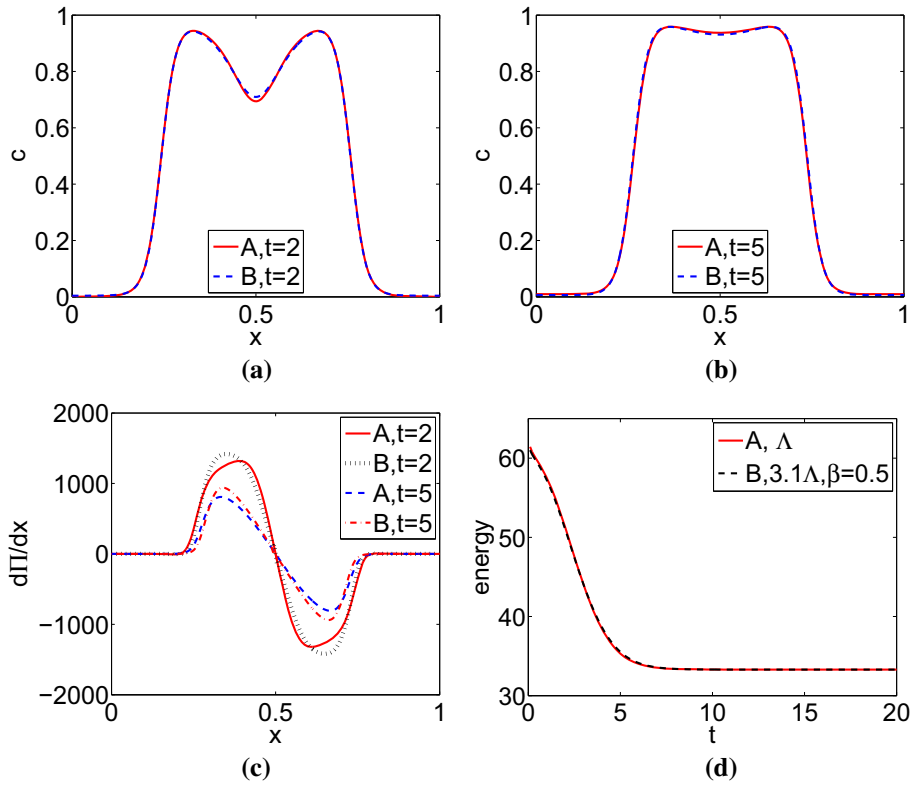

Fig. 10 Comparison of coalescent dynamics with a matched mobility. A: PFV model; B: PFM model. In the PFM model, the mobility is 3.1Λ and $\beta = 0.5$. The energy curves and the phase variables match pretty well, but not the pressure

The total energy plots with different values of parameter β are shown in Fig. 13. The energy decay process becomes slower as β increases, analogous to the scenario with the double-well potential. The total energy goes through several steps of fast decay in time; however, each of which corresponds to one coarsening process in the protuberance coalescence. There are two short plateaus and two long plateaus in the energy landscape in this case, at energy level $E^{\text{total}} = -163.07$ and $E^{\text{total}} = -197.48$, respectively. When the energy values are at the same level on the long plateaus, the states of the volume fraction are almost the same predicted by both models, as shown in Figs. 11 and 12, at time $t = 10$ and $t = 50$, respectively. But the dynamic processes in the two models are totally different in time, the knees (or steps) leading to the plateaus appear at different times in different models (see Fig. 13).

Next, we would like to match the energy curves by modifying the mobility of the PFM model as we did in the previous example. We fix $\beta = 0.5$ in the two models, $\Lambda = 5 \times 10^{-6}$ in the PFV model, and increase the mobility coefficient in the PFM model to 1.8Λ, the energy curves of the two models match well at the first knee near time $t = 3$, but not at the second knee near time $t = 18$; but if the mobility in the PFM is changed to 2.6Λ, the curves match well at the second knee near time $t = 18$, but not at the first knee near time $t = 2.5$, as shown in Fig. 14. This indicates that the simple mobility matching game that we played with the double-well potential no longer works for the more sophisticated coarsening dynamics when the Flory–Huggins potential is employed. There does not exist a suitable mobility of the PFM model such that the energy curves can match well with that of the PFV model. This indicates that hydrodynamics of the two models are fundamentally different!

6 Conclusions

We have dissected the quasi-incompressible (PFM) and the incompressible (PFV) hydrodynamic phase field model in their derivation, conservative properties, mathematical structures, linear stability and nonlinear dynamics. First, in the PFM model, the mass and momentum conservations are all enforced before the constitutive relation is determined, whereas in the PFV model, the mass conservation is enforced while the linear

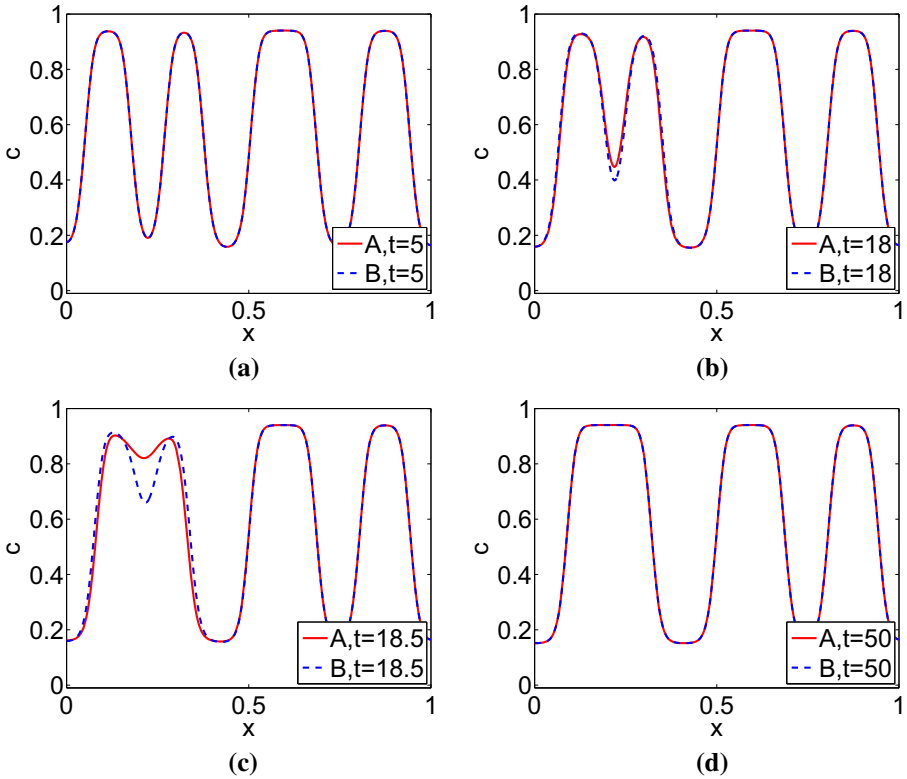

Fig. 11 Comparison of time-dependent protuberance coalescence dynamics. A: PFV model; B: PFM model. $\beta = 0.1$. Time evolution of the profiles of volume fraction c. The solutions are plotted at different times. Comparing the solutions at time $t = 18$ and 18.5, the coalescent process of the PFM model is slower than that of the PFV model. The final quasi-steady states of the two models are the same

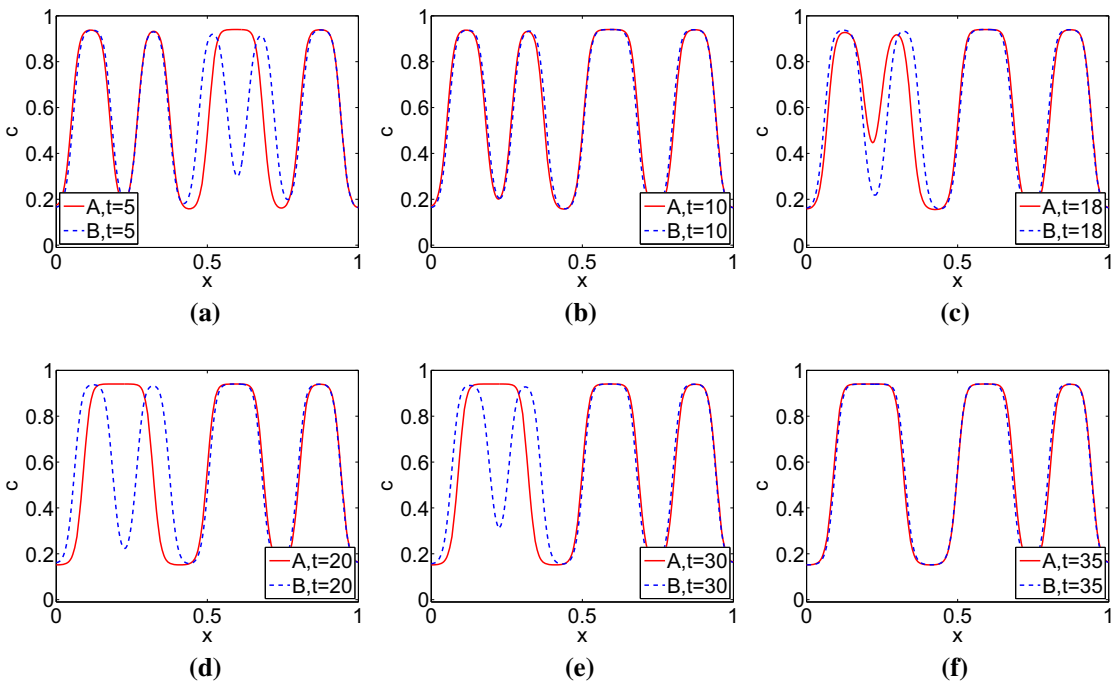

Fig. 12 Comparison of time-dependent protuberance coalescence dynamics. A: PFV model; B: PFM model. $\beta = 0.5$. Time evolution of the profiles of volume fraction c. The solutions are plotted at different times. Comparing the solutions at time $t = 18, 20, 23$ and 35, the coalescent process of the PFM model is slower than that of the PFV model. The final quasi-steady states of the two models are the same

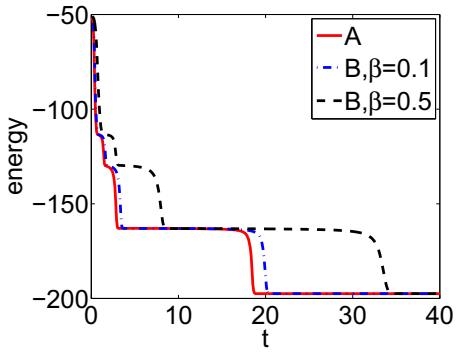

Fig. 13 Total energy curves with knees and plateaus. A: PFV model; B: PFM model

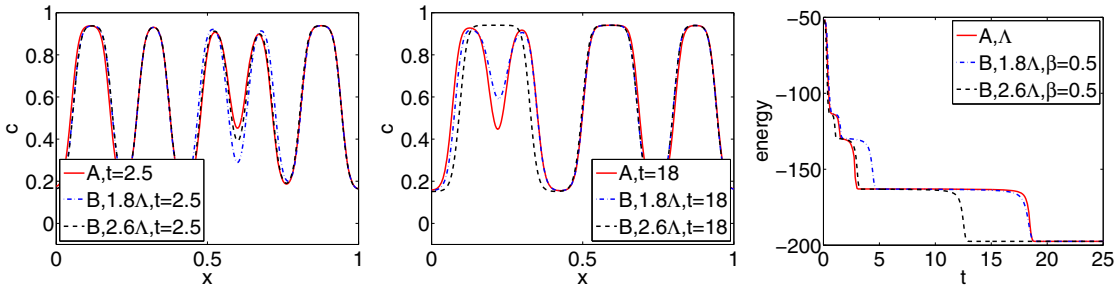

(a) **(b)** **(c)**

Fig. 14 Comparison of time-dependent protuberance coalescence dynamics with matched mobility coefficients. A: PFV model; B: PFM model. In the PFM model, $\beta = 0.5$ and the mobility is 1.8Λ or 2.6Λ

momentum conservation is not. Second, the total energy used in the two models is distinct: the kinetic energy used in the PFV model is not the real kinetic energy, because the velocity adopted is the volume-average velocity. Third, in the PFV model, the mobility coefficients for volume fractions c_2 and c satisfy $\Lambda_2 = \Lambda$; but in the PFM model, $\Lambda_2 = \Lambda(\frac{\hat{\rho}_1}{\hat{\rho}_2})^2$. Since $c + c_2 = 1$, dynamics of c and c_2 should be the same in the PFM model. The presence of the pressure in the transport equation of the phase variables in the PFM model thus must compensate for the apparent difference in the mobility inherently. Fourth, when $\frac{\hat{\rho}_1}{\hat{\rho}_2} < 1$, i.e., $0 < \beta < 1$, $\Lambda_2 < \Lambda$, the dynamic process in the PFM model is slow comparing with that in the PFV model; when $\frac{\hat{\rho}_1}{\hat{\rho}_2} > 1$, i.e., $\beta < 0$, $\Lambda_2 > \Lambda$, the dynamic process in the PFM model is fast. This is verified by our numerical simulations. In coarsening dynamics, when the energy decay only exhibits one rapid decay in time before reaching a steady state, one perhaps can adjust the mobility of one model to match the dynamics of the other; when coarsening dynamics undergoes several rapid transitions in time, as we showed with the Flory–Huggins free energy, the simple mobility matching fails to match dynamics predicted by the two models. This is a clear indication that dynamics of the two models are fundamentally different. Both models have their respective energy dissipation laws and are thereby thermodynamically consistent; PFV model does not respect the linear momentum balance while PFM does. This serves as a foundation for us to believe that the PFM model is more appropriate to use in describing dynamics of the binary fluid. A 2D numerical comparison has also been carried out by our group supporting the same conclusion [16].

Acknowledgements Xiaogang Yang's work is supported by the Scientific Research Fund of Wuhan Institute of Technology through Grants K201741; Yuezheng Gong's work is partially supported by China Postdoctoral Science Foundation through Grants 2016M591054 and the foundation of Jiangsu Key Laboratory for Numerical Simulation of Large Scale Complex Systems (201703); Jun Li's work is supported by the National Natural Science Foundation of China (Grant No.11301287), Tianjin Normal University Foundation for the introduction of talent (5RL154); Jia Zhao's work is partially supported by a Research Catalyst Grant from the Office of Research and Graduate Studies at Utah State University and Qi Wang's work is partially supported by DMS-1517347, NSFC awards #11571032, #91630207, and NSAF-U1530401.

References

1. Abels, H.: Existence of weak solutions for a diffuse interface model for viscous, incompressible fluids with general densities. Commun. Math. Phys. **289**(1), 45–73 (2009)
2. Abels, H.: Strong well-posedness of a diffuse interface model for a viscous, quasi-incompressible two-phase flow. SIAM J. Math. Anal. **44**(1), 316–340 (2012)
3. Abels, H., Garcke, H., Grün, G.: Thermodynamically consistent, frame indifferent diffuse interface models for incompressible two-phase flows with different densities. Math. Models Methods Appl. Sci. **22**(03), 1150013 (2012)
4. Aki, G.L., Dreyer, W., Giesselmann, J., Kraus, C.: A quasi-incompressible diffuse interface model with phase transition. Math. Models Methods Appl. Sci. **24**(05), 827–861 (2014)
5. Aland, S., Voigt, A.: Benchmark computations of diffuse interface models for two-dimensional bubble dynamics. Int. J. Numer. Methods Fluids **69**(3), 747–761 (2012)
6. Badalassi, V.E., Ceniceros, H.D., Banerjee, S.: Computation of multiphase systems with phase field models. J. Comput. Phys. **190**(2), 371–397 (2003)
7. Beris, A.N., Edwards, B.: Thermodynamics of Flowing Systems. Oxford University Press, Oxford (1994)
8. Borcia, R., Bestehorn, M.: Phase-field model for Marangoni convection in liquid-gas systems with a deformable interface. Phys. Rev. E **67**(6), 066307 (2003)
9. Boyer, F.: A theoretical and numerical model for the study of incompressible mixture flows. Comput. Fluids **31**(1), 41–68 (2002)
10. Chen, L.Q.: Phase-field models for microstructure evolution. Ann. Rev. Mater. Res. **32**(1), 113–140 (2002)
11. Ding, H., Spelt, P.D.M., Shu, C.: Diffuse interface model for incompressible two-phase flows with large density ratios. J. Comput. Phys. **226**(2), 2078–2095 (2007)
12. Doi, M.: Introduction to Polymer Physics. Clarendon Press, Oxford (1996)
13. Du, Q., Liu, C., Wang, X.: A phase field approach in the numerical study of the elastic bending energy for vesicle membranes. J. Comput. Phys. **198**, 450–468 (2004)
14. Du, Q., Liu, C., Wang, X.: Retrieving topological information for phase field models. SIAM J. Appl. Math. **65**(6), 1913–1932 (2005)
15. Garcke, H., Hinze, M., Kahle, C.: A stable and linear time discretization for a thermodynamically consistent model for two-phase incompressible flow. Appl. Numer. Math. **99**, 151–171 (2016)
16. Gong, Y., Zhao, J., Yang, X., Wang, Q.: Fully discrete second-order linear schemes for hydrodynamic phase field models of viscous fluid flows with variable densities. Siam J. Sci. Comput. **40**(2), B528–B553 (2018)
17. Grün, G.: On convergent schemes for diffuse interface models for two-phase flow of incompressible fluids with general mass densities. SIAM J. Numer. Anal. **51**(6), 3036–3061 (2013)
18. Grün, G., Klingbeil, F.: Two-phase flow with mass density contrast: stable schemes for a thermodynamic consistent and frame-indifferent diffuse-interface model. J. Comput. Phys. **257**, 708–725 (2014)
19. Guo, Z., Lin, P., Lowengrub, J.: A numerical method for the quasi-incompressible Cahn–Hilliard–Navier–Stokes equations for variable density flows with a discrete energy law. J. Comput. Phys. **276**, 486–507 (2014)
20. Guo, Z., Lin, P., Wang, Y.: Continuous finite element schemes for a phase field model in two-layer fluid Benard–Marangoni convection computations. Comput. Phys. Commun. **185**(1), 63–78 (2014)
21. Hua, J., Lin, P., Liu, C., Wang, Q.: Energy law preserving C^0 finite element schemes for phase field models in two-phase flow computations. J. Comput. Phys. **230**(19), 7115–7131 (2011)
22. Jacqmin, D.: Calculation of two-phase Navier–Stokes flows using phase-field modeling. J. Comput. Phys. **155**(1), 96–127 (1999)
23. Kim, J., Lowengrub, J.: Phase field modeling and simulation of three-phase flows. Interfaces Free Bound. **7**(4), 435–466 (2005)
24. Li, J., Wang, Q.: A class of conservative phase field models for multiphase fluid flows. J. Appl. Mech. **81**(2), 021004 (2014)
25. Liu, C., Shen, J.: A phase field model for the mixture of two incompressible fluids and its approximation by a Fourier-spectral method. Physica D **179**(3), 211–228 (2003)
26. Lowengrub, J.S., Ratz, A., Voigt, A.: Phase field modeling of the dynamics of multicomponent vesicles spinodal decomposition coarsening budding and fission. Phys. Rev. E **79**(3), 031926 (2009)
27. Lowengrub, J.S., Truskinovsky, L.: Quasi-incompressible Cahn–Hilliard fluids and topological transitions. Proc. R. Soc. A **454**, 2617–2654 (1998)
28. Shen, J., Yang, X.: A phase-field model and its numerical approximation for two-phase incompressible flows with different densities and viscosities. SIAM J. Sci. Comput. **32**(3), 1159–1179 (2010)
29. Shen, Jie, Yang, X., Wang, Q.: Mass and volume conservation in phase field models for binary fluids. Commun. Comput. Phys. **13**, 1045–1065 (2013)
30. Teigen, K.E., Song, P., Lowengrub, J., Voigt, A.: A diffuse-interface method for two-phase flows with soluble surfactants. J. Comput. Phys. **230**(2), 375–393 (2011)
31. Verschueren, M., Van de Vosse, F.N., Meijer, H.E.H.: Diffuse-interface modelling of thermocapillary flow instabilities in a Hele–Shaw cell. J. Fluid Mech. **434**, 153–166 (2001)
32. Wang, Q., Forest, M.G., Zhou, R.: A hydrodynamic theory for solutions of nonhomogeneous nematic liquid crystalline polymers with density variations. J. Fluid Eng. **126**, 180–188 (2004)
33. Wise, S.: Three dimensional multispecies nonlinear tumor growth—I: model and numerical method. J. Theor. Biol. **253**(3), 524–543 (2008)
34. Yue, P., Feng, J., Liu, C., Shen, J.: A diffuse-interface method for simulating two-phase flows of complex fluids. J. Fluid Mech. **515**, 293–317 (2004)
35. Zhao, J., Shen, Y., Happasalo, M., Wang, Z.J., Wang, Q.: A 3d numerical study of antimicrobial persistence in heterogeneous multi-species biofilms. J. Theor. Biol. **392**, 83–98 (2016)

36. Zhao, J., Wang, Q.: Modeling cytokinesis of eukaryotic cells driven by the actomyosin contractile ring. Int. J. Numer. Methods Biomed. Eng. **32**(12), e2774 (2016)
37. Zhao, J., Wang, Q., Yang, X.: Numerical approximations to a new phase field model for two phase flows of complex fluids. Comput. Methods Appl. Mech. Eng. **310**, 77–97 (2016)